Naval Research Laboratory
Washington, DC 20375-5000

NRL Memorandum Report 6057

Characterization of PEOS Plasma Parameters and Conduction Phase Properties

R. J. COMMISSO, D. D. HINSHELWOOD,* J. M. NERI,
W. F. OLIPHANT, AND B. V. WEBER*

Plasma Technology Branch
Plasma Physics Division

**Jaycor, Vienna, VA*

December 31, 1987

SECURITY CLASSIFICATION OF THIS PAGE

REPORT DOCUMENTATION PAGE

Form Approved
OMB No 0704-0188

1a REPORT SECURITY CLASSIFICATION UNCLASSIFIED	1b RESTRICTIVE MARKINGS
2a SECURITY CLASSIFICATION AUTHORITY	3 DISTRIBUTION / AVAILABILITY OF REPORT Approved for public release; distribution unlimited.
2b DECLASSIFICATION / DOWNGRADING SCHEDULE	
4 PERFORMING ORGANIZATION REPORT NUMBER(S) NRL Memorandum Report 6057	5 MONITORING ORGANIZATION REPORT NUMBER(S)
6a NAME OF PERFORMING ORGANIZATION Naval Research Laboratory 6b OFFICE SYMBOL (If applicable) Code 4770	7a NAME OF MONITORING ORGANIZATION
6c ADDRESS (City, State, and ZIP Code) Washington, DC 20375-5000	7b ADDRESS (City, State, and ZIP Code)
8a NAME OF FUNDING / SPONSORING ORGANIZATION ONR, DOE & DNA 8b OFFICE SYMBOL (If applicable)	9 PROCUREMENT INSTRUMENT IDENTIFICATION NUMBER
8c ADDRESS (City, State, and ZIP Code) DOE - Washington, DC 20545 DNA - Washington, DC 20305	10 SOURCE OF FUNDING NUMBERS PROGRAM ELEMENT NO: (See p. ii) PROJECT NO: (See p. ii) TASK NO: (See p. ii) WORK UNIT ACCESSION NO: (See p. ii)

11 TITLE (Include Security Classification)
Characterization of PEOS Plasma Parameters and Conduction Phase Properties

12 PERSONAL AUTHOR(S)
Commisso, R.J., Hinshelwood,* D.D., Neri, J.M., Oliphant, W.F., and Weber,* B.V.

13a TYPE OF REPORT	13b TIME COVERED	14 DATE OF REPORT (Year, Month, Day)	15 PAGE COUNT
Interim	FROM 1/82 TO 12/86	1987 December 31	70

16 SUPPLEMENTARY NOTATION
*Jaycor, Vienna, VA

17 COSATI CODES			18 SUBJECT TERMS (Continue on reverse if necessary and identify by block number)
FIELD	GROUP	SUB-GROUP	PEOS plasma characterization Current conduction process

19 ABSTRACT (Continue on reverse if necessary and identify by block number)

This report is a compilation and summary of data, previously presented in numerous and disparate forums, that characterize the initial plasma parameters and conduction phase of the plasma erosion opening switch. The results verify the approximate values of the parameters used in modeling the switch and support the current controlled erosion switch theory.

20 DISTRIBUTION / AVAILABILITY OF ABSTRACT	21 ABSTRACT SECURITY CLASSIFICATION
☒ UNCLASSIFIED/UNLIMITED ☐ SAME AS RPT ☐ DTIC USERS	UNCLASSIFIED
22a NAME OF RESPONSIBLE INDIVIDUAL Robert J. Commisso	22b TELEPHONE (Include Area Code) (202) 767-2468 22c OFFICE SYMBOL Code 4770.2

DD Form 1473, JUN 86 Previous editions are obsolete SECURITY CLASSIFICATION OF THIS PAGE

SECURITY CLASSIFICATION OF THIS PAGE

10. SOURCE OF FUNDING NUMBERS

	PROGRAM ELEMENT NO.	PROJECT NO.	TASK NO.	WORK UNIT ACCESSION NO.
DOE			DE-AI08-79DP40092	DN680-382
DNA	62715H		T99QAXLA-00038	DN320-094

DD Form 1473, JUN 86 (Reverse)

CONTENTS

CHARACTERIZATION OF PEOS PLASMA PARAMETERS AND CONDUCTION PHASE PROPERTIES

I. INTRODUCTION:

The plasma erosion opening switch (PEOS) is a fast, high power, vacuum opening switch which can be used in a variety of configurations for opening switch power conditioning applications.[1] Plasma is injected, in vacuum, between the electrodes of a generator, or driver, previous to the arrival of the power pulse, and physically just before the load and after the previous power conditioning stages. The plasma acts as a short circuit on one time scale and then opens on a much shorter time scale, generating high voltage and delivering a higher power pulse to the load than could otherwise be expected.

Compiled and summarized in this report are data, previously presented in numerous and disparate forums, that characterize the initial plasma parameters and the conduction phase of the PEOS. Of particular importance is the estimated value of the plasma density (including the effect of plasma wall interactions) and ion collection rate used by the Naval Research Laboratory (NRL) in obtaining agreement between the current controlled (magnetic field penetration) PEOS model and observations from experiments. Also of interest are results of experiments investigating the parametric dependencies of the switch conduction current and characterizing the magnetic field (and inferred current) distribution in the switch. There are several experimentally observed properties that uniquely characterize the conduction and opening phase of the PEOS. Among these are the time delay control of the maximum switch conduction current, the broad, predominately radial current channel, the characteristic fast opening, and the transition from fast opening to slow opening. The most useful PEOS model must self-consistently account for these properties while being

Manuscript approved August 21, 1987.

consistent with the best estimate of the PEOS plasma parameters. Thus, building a credible data base in this area is crucial.

Data concerning the characterization of the initial injected plasma, including plasma-surface interactions, obtained from test stand and in situ measurements are found in Sec. II. In Sec. III, we present data that describe the conduction phase of the PEOS and relate them to the measurements described in Sec. II and the current controlled PEOS model. The current conduction process is characterized through measurements of the internal magnetic field distribution. The work is summarized in Sec. IV.

II. PEOS PLASMA CHARACTERIZATION:

A. Test Stand Results:

A test apparatus was assembled consisting of a single, Mendel type plasma gun[2] and simulated planar switch electrodes. A schematic of the experiment is shown in Fig. 1. The electrodes were made up of a 70-80% optically transmitting brass screen and an Aerodag coated aluminum plate. The relative spacings in the x direction (Fig.1) were chosen to be identical to those in the radial direction of the cylindrical geometry used in Gamble I experiments.[1,3,4] In Gamble I the radial separation between the cylindrical inner (cathode) and outer (anode) conductors was 2.5 cm and the radial separation between the plasma source and cathode was 10 cm. The apparatus was evacuated to $\simeq 5 \times 10^{-4}$ torr, very similar to the Gamble I experiments. The capacitor driving the gun (0.6 μF) was in the standard "doghouse" configuration[2] at an initial voltage of 25 kV. The current into the gun reached ≃ 40 kA in ≃ 0.5 μs.

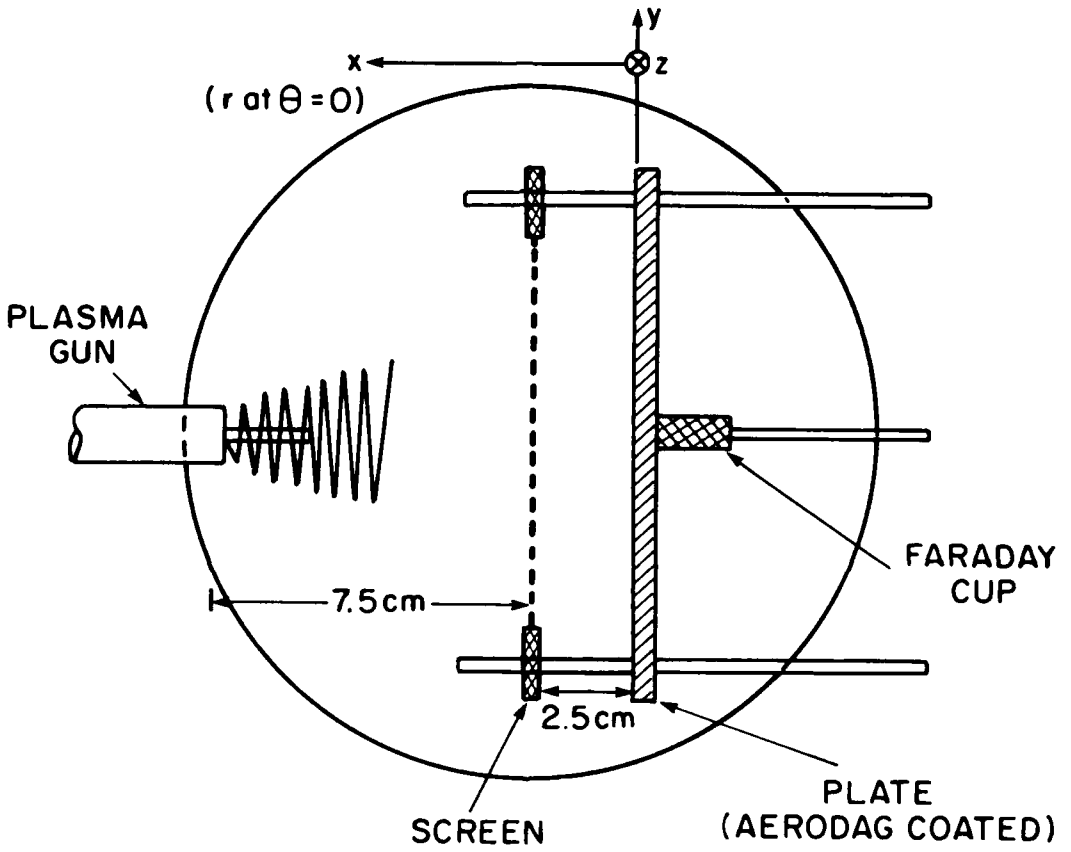

Fig. 1 Schematic of test stand apparatus for measurement of plasma parameters.

1. Time Resolved Photography.[5]

As illustrated in the upper portion of Fig. 2, a framing camera was set up to view the plasma injection region from the side. A sequence of these side viewing framing camera photographs each having 100-ns exposure is shown in the central portion of Fig. 2. The lower portion of Fig. 2 is the signal from a Faraday cup located behind the plate on the axis of the system. Throughout Sec. II, time is measured from the initiation of the gun current.

Visible light does not appear on the plate (cathode) until $t \simeq 1.65$ μs. This is consistent with gun injected plasma speed of $\simeq 6$ cm/μs. There is no luminosity observed from the inter-electrode region at this time and exposure level. We estimate from the photos that at $t \simeq 2.2$ μs, the light at the cathode extends into the inter-electrode region ≃ 10% of the plate screen (cathode-anode) separation, which corresponds to ≤ 0.2 cm of emitting plasma. At $t > 2.2$ μs both electrodes are quite luminous and some weak emission appears from the inter-electrode region. Data from PEOS experiments[1,3] indicate that fast switching deteriorates rapidly when Gamble I is fired at $t > 2.2$ μs. The Faraday cup signal shown in Fig. 2 is well past peak and near zero at $t \geq 2.2$ μs.

An illustration of the setup used for side viewing steak photography with the test stand apparatus is shown in the upper portion of Fig. 3. Two streak records at different sweep rates, one slow (≃ 7-μs full sweep) and the other fast (≃ 3-μs full sweep), are displayed in the central portion of Fig. 3. The Faraday cup signal is shown again for reference in the lower portion of the figure. The gun generated plasma front has an apparent speed of 5-6 cm/μs. At $t \geq 2$ μs a weakly luminous front appears

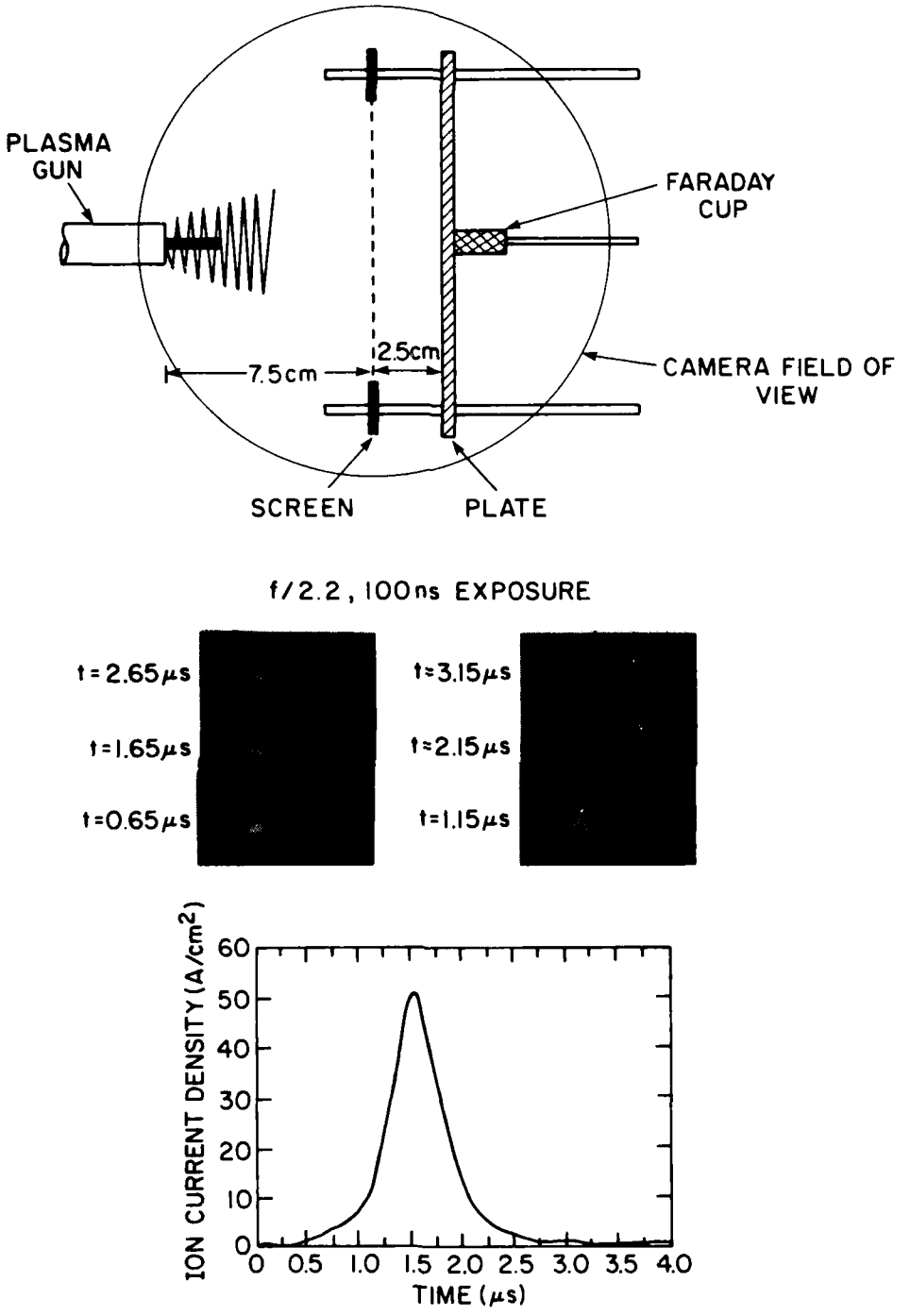

Fig. 2 Upper: Illustration of framing camera field of view for test stand experiments. Middle: Sequence of framing camera photographs. Lower: Faraday cup signal.

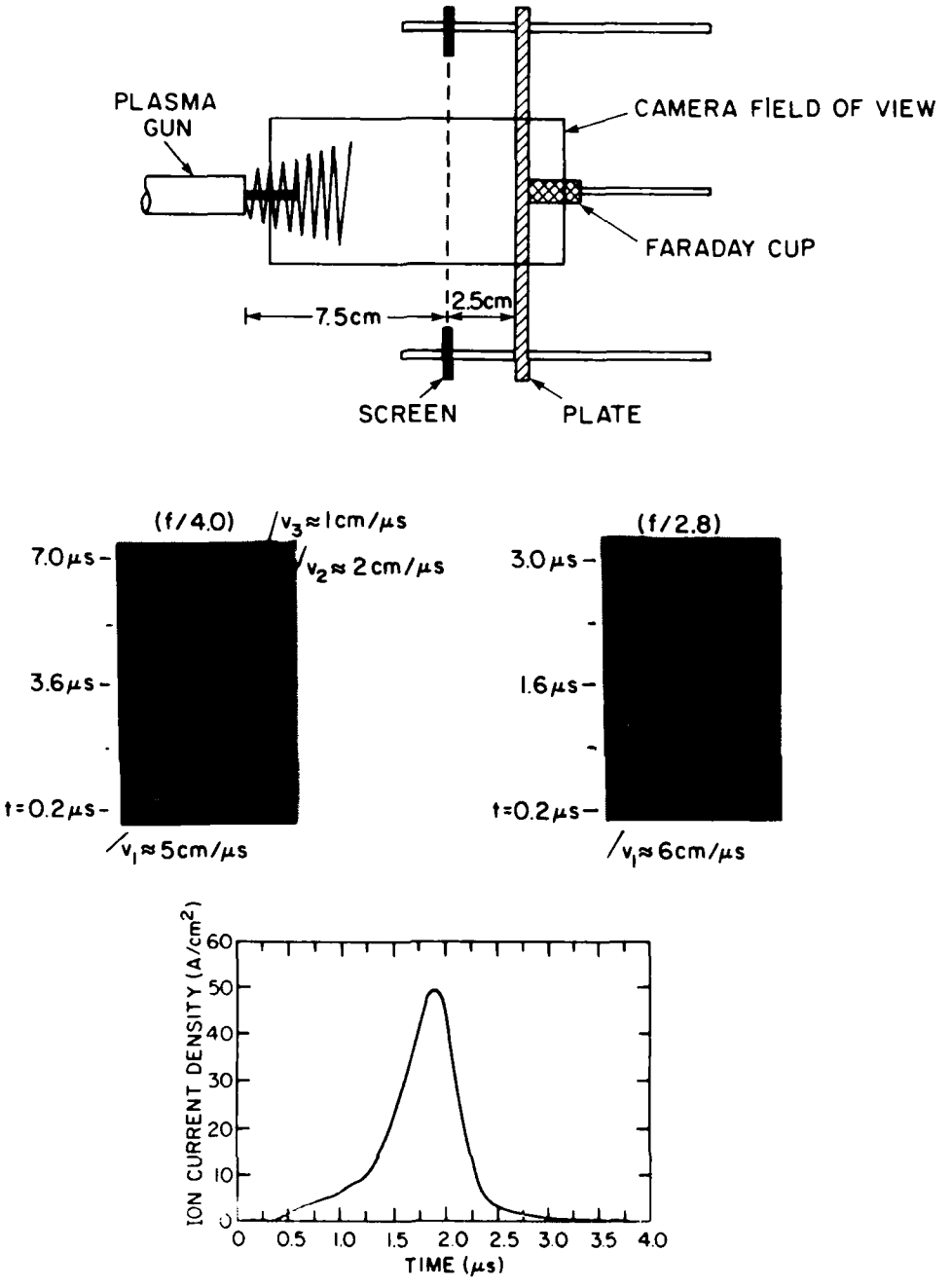

Fig. 3 Upper: Illustration of streak camera field of view for test stand experiments. Middle: Two streak photographs with different time sweeps. Lower: Faraday cup signal.

to move off the screen (anode) at a speed of 1-2 cm/μs. The region of high luminosity at the electrode surfaces occupies $\leq$ 10% of the inter-electrode spacing ($\leq$ 0.2 cm) at t $\simeq$ 2 μs and then expands at a speed $\leq$ 1cm/μs. These results are all consistent with the framing camera photographs in Fig. 2. Again, it is important to note that fast switching is observed[1,3] if Gamble I is fired when t $\leq$ 2.2 μs. After this time, the relative light emission from the surfaces increases, the Faraday cup signal decreases and the switching action degrades.

2. Spectroscopy.

The same apparatus described above was used to make both time integrated[5] and time resolved[6] spectroscopic measurements. The experimental arrangement is illustrated in Fig. 4 with the relative spacings between the gun, screen, and plate identical to what is shown in Fig. 1. The entrance slit of the 0.5-m monochromater and lens were adjusted to observe light from a 1-mm wide cross section of the plasma and the mirror could be adjusted to select any line-of-sight parallel to, and between, the plate and screen. The exit slit of the monochromater was chosen to only allow light from a single spectral line to be observed. The line emission was recorded using a photomultiplier operated in its linear response range. A relative calibration of the monochromater-photomultiplier system was performed. Depending on the region of the spectrum, the system sensitivity could change by a factor of ~ 6 over a range of $\leq$ 500 Å.

If $N^Z(u)$ represents the density of ions (cm^{-3}) of charge state Z in the upper (excited) state, u, of an atomic transition, u$\Rightarrow$l

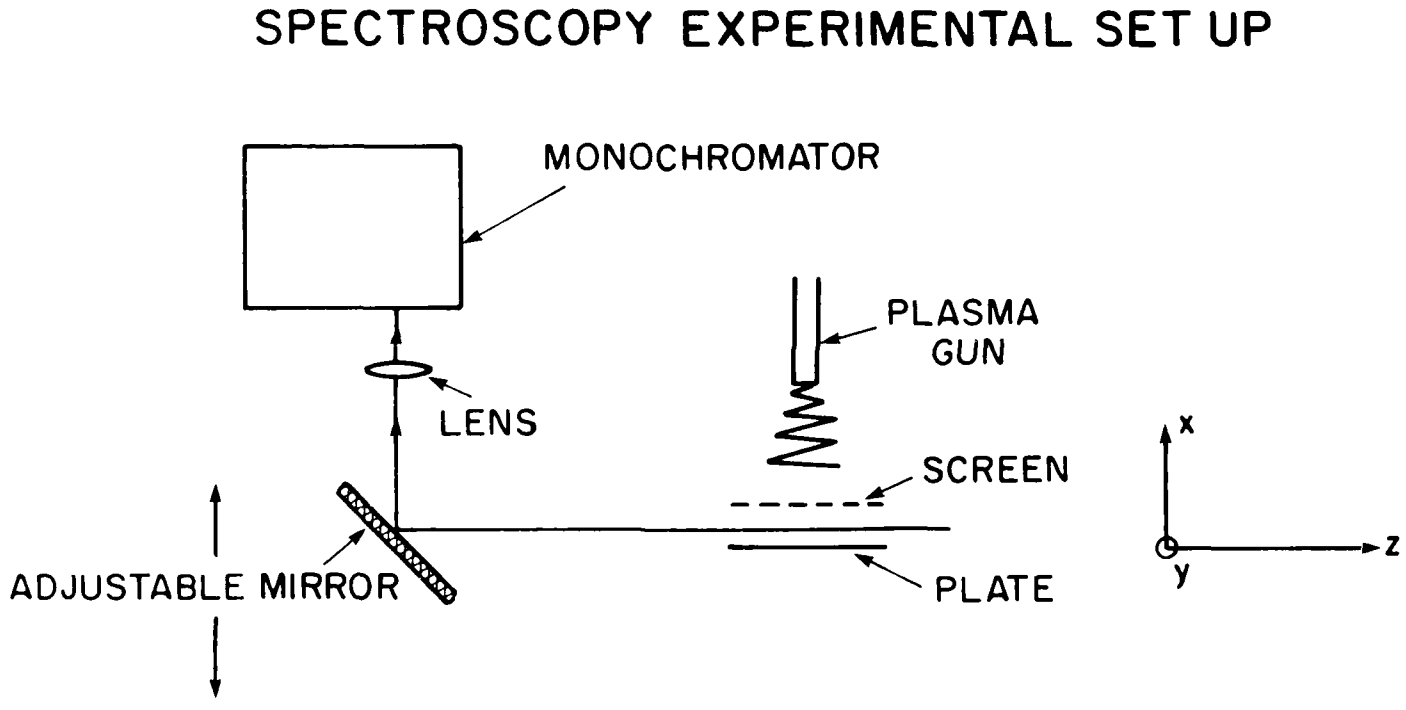

Fig. 4 Schematic of setup for spectroscopic measurements.

(where 1 represents the lower state of the transition), then the emission coefficient, ε, is given by

$$\varepsilon = \frac{\Delta E_{ul}}{4\pi} A_{ul} N^Z(u) \left[\frac{\text{watts}}{\text{cm}^3\text{-sterad}}\right] , \qquad (1)$$

where ΔE_{ul} is the energy emitted in the transition (joules) and A_{ul} is the transition probability (sec^{-1}). For optically thin lines, the monochromater measures the integral of ε along the line-of-sight. Depending on the plasma conditions, models[7] can be assumed for both the relationship between $N^Z(u)$ and $N^Z(g)$, the density of ions of charge state Z in the ground (unexcited) state, and the relationship between the ground state densities of ions of various charge states. For example, in an equilibrium corona model,[7] which is appropriate for many low density ($\leq 5 \times 10^{14}$ cm^{-3}), high temperature (≥ 1 eV) plasmas, collisional ionization and excitation by electrons are balanced by radiative recombination and decay, respectively. Thus, it can be shown[7] that for a plasma in which a coronal equilibrium exists

$$\frac{N^Z(g)}{N^{Z+1}(g)} = \frac{\alpha(T_e, Z+1, g)}{S(T_e, Z, g)} , \qquad (2)$$

and

$$\frac{N^Z(u)}{N^Z(g)} = n_e \frac{X_{gu}(T_e)}{\sum_{j<u} A_{ju}} , \qquad (3)$$

where α, S, and X are the radiative recombination, collisional ionization, and collisional excitation rate coefficients, respectively, T_e is the electron temperature, and n_e is the electron density (also known as the plasma density). The sum in Eq.(3) is over all states $j < u$. The units of α, S and X are cm^3/sec. As can be seen from Eqs. (1)-(3), the plasma properties (density and temperature) and the relative ion density in a

given charge state are highly interrelated. Moreover, the relationship is very model dependent.

A more complete analysis of the distribution of excited states and charge species can be obtained from the collisional-radiative (CR) model.[7] Here, more atomic excitation, relaxation, ionization, and recombination processes are included and the problem rapidly becomes untractable analytically. Numerical calculations using the CR model were performed[8] for a carbon plasma in equilibrium, having ion densities of $n_i = 10^{13}$ cm^{-3}, 10^{14} cm^{-3}, and 10^{15} cm^{-3} and at $T_e = 1,3,5,7$ and 10 eV for each density. By comparing predicted line intensity ratios with the observed ratios, T_e and n_e can be roughly bracketed, assuming a pure carbon plasma in CR equilibrium and recognizing the model has a necessarily finite nature (i.e. all possible transitions and processes are not included). Note that because of the uncertainties involved in the calculations, the temperatures and densities inferred in this manner only can be used to support other, more direct measurements.

Initial experiments were performed with no screen or plate in the system. Time resolved measurements of emission from CI (2478.6 Å), CII (2837.0 Å),CIII (2296.9 Å), and H_β (4861.3 Å) indicated that under these conditions, only the CIII (doubly ionized carbon) radiation could be observed during any reasonable time of interest ($\leq$ 5 μs). We conclude this on the basis of not being able to observe radiation from the other species even when the sensitivity of the measurement was increased by a factor $\geq$ 50. This observation was confirmed by time integrated spectroscopy, which showed little or no emission from other carbon charge states or other plasma species unless the screen was present. From these results one can conclude that the plasma ejected from the gun is primarily C^{++} and possibly protons (no measurements of protons were attempted). As described in what

follows, similar data taken with the screen and plate indicate emission from other species near the surfaces, but only for $t > 1.5$ μs. For times of interest, $t < 2$ μs, the emission from the region between the surfaces does not differ significantly from the case with no surfaces present.

Based on the numerical calculations using the CR model and the measured relative line strengths we estimate that 10^{13} cm $^{-3} \leq n_i \leq 10^{14}$ cm^{-3} and 4 eV $\leq T_e \leq$ 8 eV. Over this range the model predicts $\geq$ 80% of the carbon is doubly ionized, i.e., C^{++}. Because $n_e = \langle Z \rangle n_i$, where $\langle Z \rangle$ is the effective ion charge state, the average electron density for the gun produced plasma ranges 2×10^{13} cm$^{-3} \leq n_e \leq 2 \times 10^{14}$ cm^{-3}. Analytical estimates of the relevant atomic rate processes for these conditions imply that for the gun produced plasma alone, the ionization equilibrium is "frozen-in." That is, when the plasma is produced, or very soon after, the relative densities of ions in various charge states reach an equilibrium that stays fixed for many tens of microseconds. The temperature and density were independently measured to be ~ 5 ev and ~ 5 x 10^{13} cm^{-3} (see Sec. II. A. 3 -4), for which the equilibrium CR calculation predicts that > 80% of the carbon is doubly ionized.

In Fig. 5, the time history of the emission from the 2296.9 Å line of CIII, measured with and without the screen, is shown at x≈ 2.4 cm (see Fig. 1). With the screen present, the initial intensity is ≈ 30% lower, probably a result of the finite screen transparency. However, the emission increases rapidly at $t > 1.5$ μs, indicating some kind of plasma-wall interaction phenomenon near the screen. It is at this time (or shortly after) that the streak and framing camera photography indicate enhanced light emission from the screen and plate.

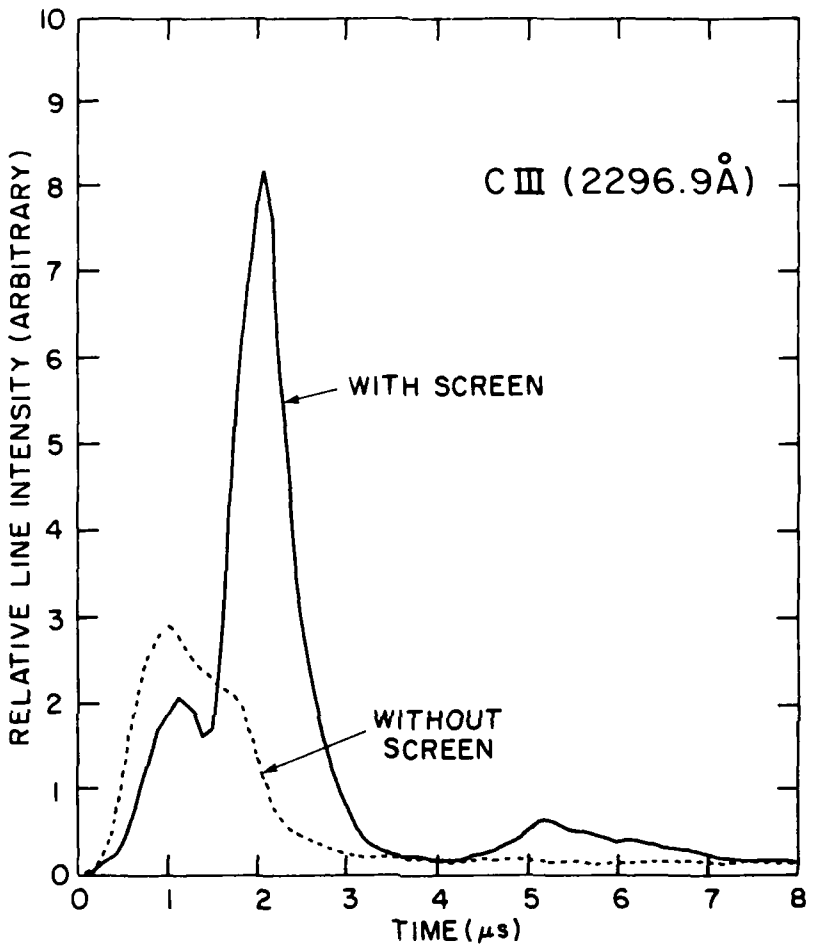

Fig. 5 Time history of CIII (2296.9 Å) spectral line comparing emission with and without screen.

A compilation of the line emission data with surfaces is shown in Fig. 6. Here the CI, CII and CIII emission lines as well as emission from H_β (neutral hydrogen) are compared at three inter-electrode positions as a function of time. At $t \leq 1.5$ μs, there is significant CIII emission everywhere, but no emission from the other carbon species and, as described earlier, no emission is observed from these species when no screen is present. At $t \simeq 1.5$ μs, emission from CII, CI and H_β appears from both the screen and plate at roughly the same time. (Note that at a drift speed of ≥ 7 cm/μs, the gun produced plasma only takes ≤ 350 ns to cross the inter-electrode gap.) Clearly, the observed emission from CII, CI and H_β is a result of the presence of the metal surfaces. No significant emission is observed from CII, CI or H_β at the intermediate position ($x = 1.5$ cm) for another 0.5 - 0.75 μs. Thus, the ions with $Z < 2$ that are created as a result of the interaction of the gun generated plasma with the walls diffuse into the region between the electrodes at an effective speed of $\simeq 1$ cm/μs (assuming diffusion occurs from both surfaces). This result is consistent with the streak and framing camera photography.

The results of the CR model numerical calculations for this case indicate that for $t \geq 2.5$ μs, at the measurement locations nearest the surfaces, the ion density has increased slightly to $n_i \simeq 10^{14}$ cm^{-3} and the electron temperature has fallen to $T_e \leq 1$ eV. Under these conditions, the plasma is predominately CII so that $\langle Z \rangle = 1$ and $n_e \simeq n_i$. For times of interest ($t \leq 2$ μs) in the region between the surfaces, the conditions are very similar to those observed with no surfaces present, which implies n_e and T_e are roughly the same as they are when no surfaces are present. Note that here the validity of the assumption of equilibrium used in the CR model is highly questionable, particularly in the transient situation of the injected plasma interacting with the surfaces.

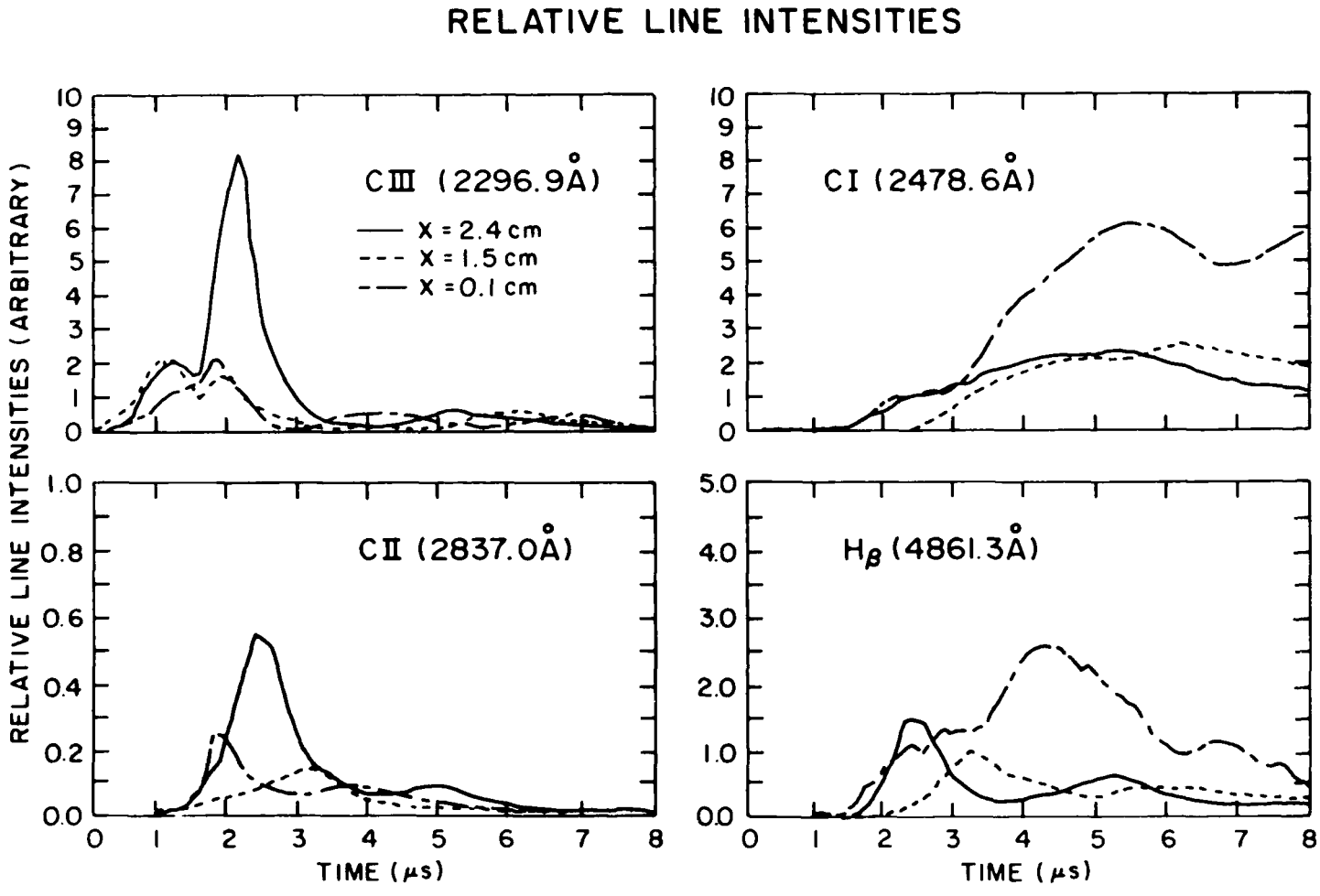

Fig. 6 Time histories of CIII (2296.9 Å), CII (2837.0 Å), CI (2478.6 Å), and H_β (4861.3 Å) spectral lines at three locations.

We summarize the results of the visible photography and spectroscopy as follows: The gun injected ions are predominately carbon with an effective charge of $\langle Z \rangle \simeq 2$. The proton fraction has not been determined. If the gun injected plasma was in CR equilibrium the average electron temperature and density would be $T_e \simeq 6$ eV and $n_e \simeq 7 \times 10^{13}$ cm^{-3}. No neutral carbon radiation is observed. The temperature and density were independently measured to be in the range of ~ 5 ev and ~ 5×10^{13} cm^{-3} (see Sec. II. A. 3-4). The equilibrium CR calculations for these parameters predict that > 80% of the carbon is doubly ionized. When surfaces are present, the bulk of the plasma between the screen and plate remains unchanged for $t < 2$ μs. As a result of plasma-wall interactions, lower charge state carbon (CI and CII) and hydrogen evolve from the surfaces after $t \simeq 1.5$ μs. These species then drift into the region between the screen and plate at an effective speed of ≃ 1 cm/μs. Based on the CR equilibrium calculations, we speculate that for $t \geq 2.5$ μs, at ≃ 0.2 cm from the screen and plate, $n_e \simeq 10^{14}$ cm^{-3} and $T_e \leq 1$ eV.

3. Microwave Measurements.

Microwaves are commonly used to measure electron density in plasmas.[9,10] This method is desirable because it is non-perturbing and independent of plasma flow velocity, temperature, and other parameters. Transmission and interferometric measurements were attempted using the test stand described earlier. The general arrangement is shown in Fig. 7. A carbon plasma gun injects plasma between two microwave horns. No additional surfaces or screens were used in these measurements. The sending horn is powered by a Klystron tube that produces microwaves of

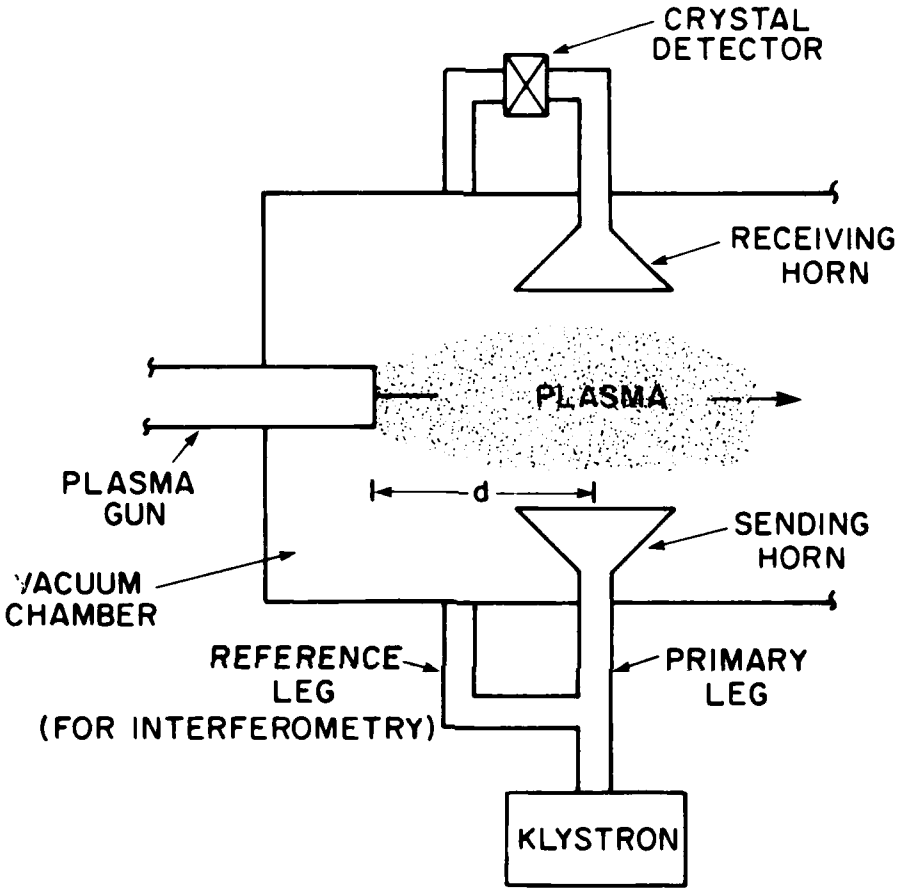

Fig. 7 Schematic of set up for microwave measurements of plasma density.

4.3-mm wavelength (70-GHz frequency) The Klystron provides continuous microwave radiation at a power level of a few 100 mW. The receiving horn collects a fraction (<10%) of the incident energy and the power received is monitored with a crystal detector. This is the simple arrangement used for transmission measurements. Alternatively, the detected microwaves that tranverse the plasma can be added to those detected from a reference leg (i.e., microwaves that traverse a known path that does not intersect the plasma) to form a interferometer. The power in the summed waves is monitored by a detector for interference measurements.

Microwaves travel through a plasma with little attenuation as long as the electron density is below a critical value, n_c. This critical density is found by equating the electron plasma frequency to the microwave frequency:

$$n_c = 1.24 \times 10^{-8} f^2 = 1.12 \times 10^{13}/\lambda^2, \qquad (4)$$

where f(Hz) and λ(cm) are the microwave frequency and wavelength, respectively. Microwaves will propagate through the plasma with little attenuation (reflection) if $n_e < n_c$. For the source used here, $\lambda = 0.43$ cm and $n_c = 6 \times 10^{13}$ cm^{-3}. When $n_e > n_c$, the microwaves are said to be "cut off." This is the principle behind the transmission measurements. The received signal goes to zero when the density somewhere between the horns exceeds n_c (6×10^{13} cm^{-3}). Transmission resumes as the density decays away and $n_e < n_c$. Limited information can be gained by inspecting the signals before or after cutoff using this measurement technique.

The transmitted power was measured for two cases: d = 20 cm and d = 10 cm (10 cm being the "standard" operating distance in PEOS

experiments[2,3]). Sample data are shown in Fig. 8(a) (at 5 μs/div) and Fig. 8(b) (at 1 μs/div) for d = 20 cm. Full power (no plasma) corresponds to 1.0 and zero power (no microwaves) corresponds to zero on these traces. The gun current is shown in Fig. 8(c) for timing purposes. As can easily be seen, the microwaves are cut off between 4 and 5 μs after the initiation of the gun current. The peak density remains above 6×10^{13} cm^{-3} for $5\ \mu s \leq t \leq 15\ \mu s$. Some effects from the presence of plasma are evident for 40 μs. With the gun moved closer to the horns, cutoff occurs earlier, as would be expected. Sample data with d=10 cm are shown in Fig. 9. They indicate cutoff 2.5 μs after the start of the gun current (the initiation of the gun current was at t = 2 μs on this figure). This agrees with the crude spectroscopic estimates discussed earlier. The peak density stays above 6×10^{13} cm^{-3} for at least the next 6 μs. The time response of the detectors is too slow to follow changes faster that ≃ 1 μs so the signals shown in Figs. 8 and 9 can not show any faster time dependence of the microwave power.

Interferometry can be used to measure n_e as a function of time for $n_e < n_c$. The microwaves associated with the primary leg are added to those of a "reference leg," which is tapped off the primary leg before traversing the plasma (see Fig. 7). The phases of the two waves are adjusted so that when no plasma is present they add (constructive interference) and the magnitudes are adjusted so that they are equal. The presence of the plasma will introduce a phase shift in the primary leg. For example, a 180^o phase shift in the received waves will cause total destructive interference. Thus, power detected will vary with time as the

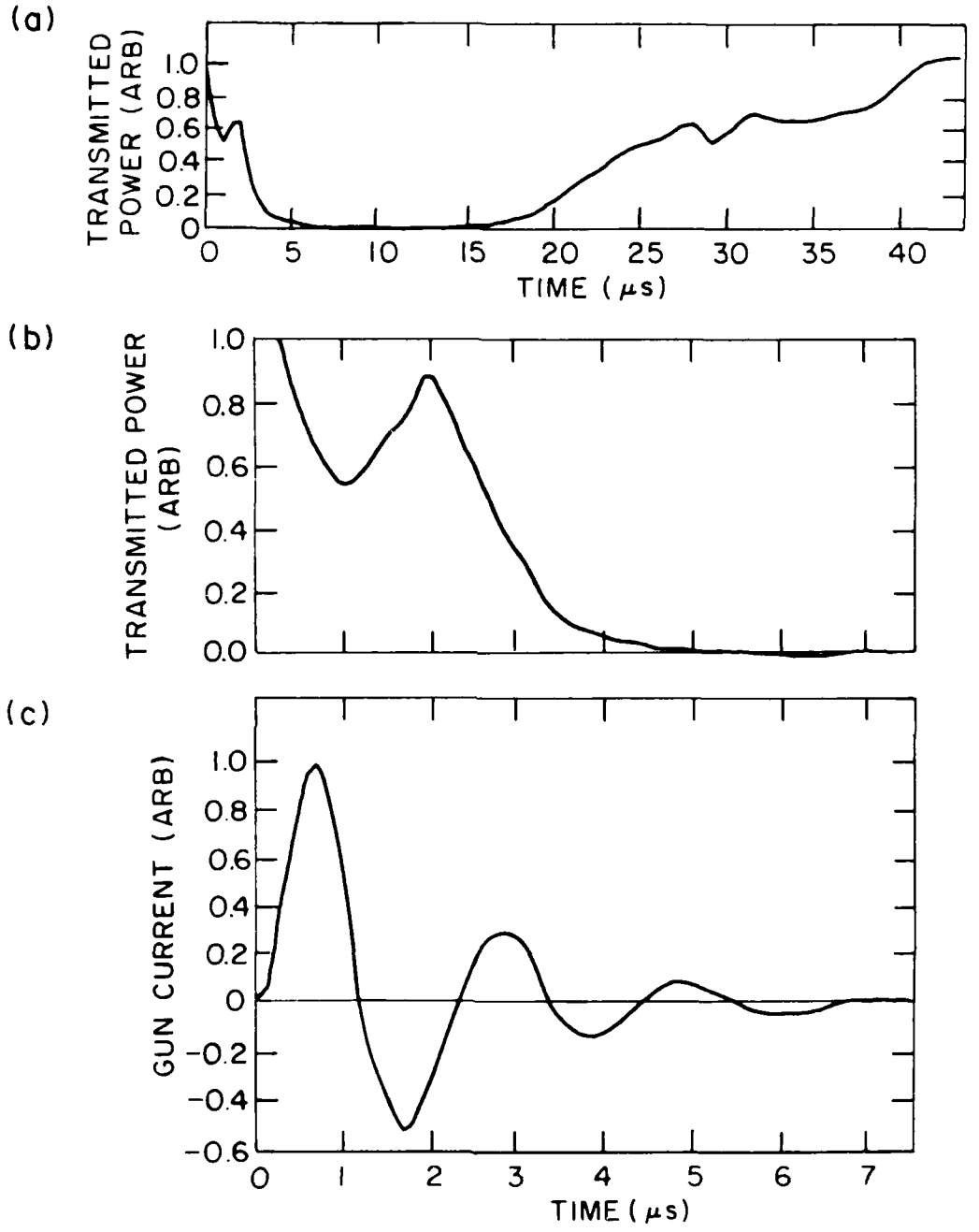

Fig. 8 Illustration of microwave cutoff measurements at d=20cm. The plasma density is > 6×10^{13} cm^{-3} at t ≈ 5 μs.

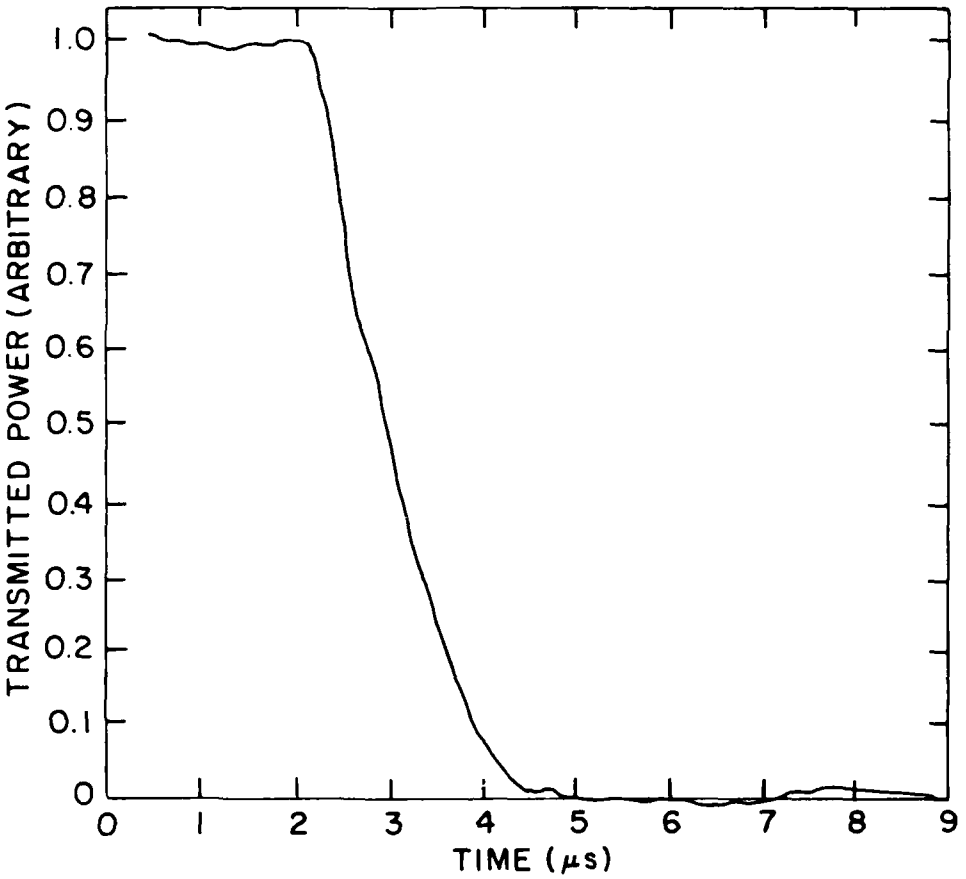

Fig. 9 Illustration of microwave transmission measurements at d=10 cm. The plasma density is $> 6 \times 10^{13}$ cm^{-3} at $t \simeq 2.5$ μs (here, gun current starts at $t = 2.0$ μs).

density between the horns changes. The phase change for microwaves traversing a length L of plasma is given by:

$$\Delta\phi = \simeq \frac{2\pi}{\lambda} \int_0^L \left[1 - (1 - \frac{n_e(x)}{n_c})^{1/2}\right] dx \simeq \frac{\pi}{\lambda n_c} \int_0^L n_e(x)dx, \qquad (5)$$

where dx is an elemental length along L and we assumed $n_e << n_c$. By analyzing the interference signal one can obtain $\Delta\phi$. Then n_e can be determined from Eq. (5) if the spacial variation of n_e is known.

Here, the interferometer uses one detector to measure the power in the summed waves from the reference leg and primary leg (Fig. 7). The primary microwaves have amplitude B(t) and phase change $\Delta\phi$ from the plasma. The power in the summed waves is then

$$P \propto A^2 + B(t)^2 + 2AB(t) \cos [\Delta\phi(t)], \qquad (6)$$

where A is the amplitude of the reference microwaves and B(t=0) = A. If B(t) is constant(= A), the detected power will oscillate between a maximum value of $4A^2$ and a minimum of 0 as $\Delta\phi$ changes from 0 to π. In the actual experiment B is a strong function of time (e.g., for $n_e > n_c$, B = 0).

Results with a single detector are shown in Fig. 10 for d = 10 cm at 1 μs/div and 10 μs/div. When the microwaves are cutoff, B = 0 and $P \propto A^2$. This occurs between t = 3 and 20 μs. There should be many oscillations between t = 2 and 3 μs as the density builds up to 6×10^{13} cm^{-3}, but the detector cannot follow the rapid density variation because of its limited time response (as discussed above). When the density

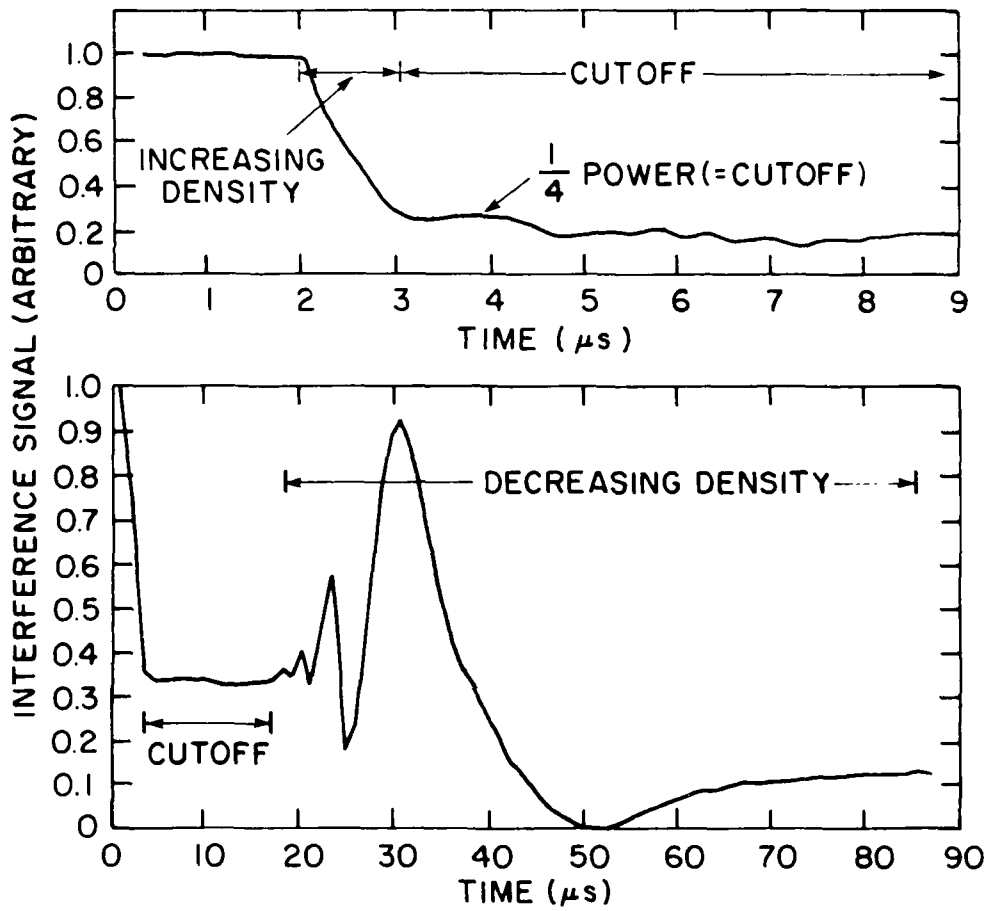

Fig. 10 Illustration of microwave interference measurements at d = 20 cm. Fringes associated with increasing density for 2 μs > t > 3 μs cannot be resolved because of slow detector response.

decays ($n_e < 6 \times 10^{13}$ cm^{-3}), oscillations are seen on the slow time sweep for $t > 20$ μs. Each maximum and minimum corresponds to a change in $\Delta\phi$ of 180^o (so-called "fringes"). For future measurements, better time response is required to monitor density changes in the first 2 μs and more detector channels are needed to unambigiously determine if $\Delta\phi$ is increasing or decreasing.

To "slow down" the density time dependence, the gun-horn distance was increased to d = 60 cm. Interference signals are shown in Fig. 11 at 1 μs/div and 10 μs/div. The detector time response was improved by lowering the termination resistance, but this also decreased the sensitivity. The 1 μs/div trace shows a 180^o phase shift 3 μs after the start of the gun current, corresponding to an average density of 2×10^{12} cm^{-3} over a length of 12.5 cm (the diameter of the aperture) for a plasma moving at ≈ 15-20 cm/μs. After 7 μs, the density is about 4×10^{12} cm^{-3}, etc. The 10 μs/div trace shows the density rise and decay for 60 μs. The peak density is probably at t = 15 μs, the second minimum of the interference signal. A second detector sensitive to $\sin(\Delta\phi)$ is needed to accurately determine $\Delta\phi$.

In summary, the microwave transmission measurements yield $n_e \geq 6 \times 10^{13}$ cm^{-3} when $t \geq 2.5$ μs, 10 cm from the gun. This is supported by the spectroscopic data. The density (somewhere in the line of sight of the microwaves traversing the plasma) remains $\geq 6 \times 10^{13}$ cm^{-3} for 15-20 μs. Although an interference signal has been detected, the measurement technique must be refined to obtain better data. Time resolved density determination using interferometer techniques will be possible with more and faster detectors. (Note in passing that the Faraday cup signal is usually zero at $t > 2$ μs.)

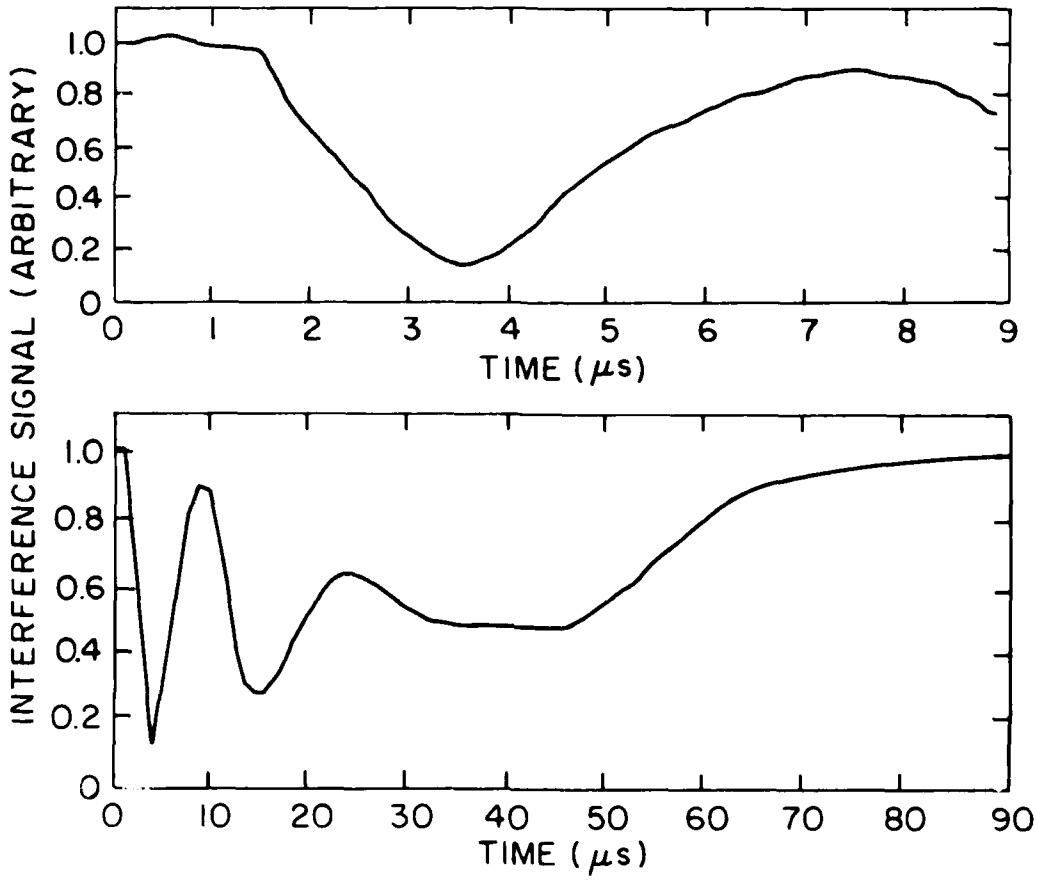

Fig. 11 Illustration of microwave interference measurements at d = 60 cm. The time variation of n_e is much slower at this large separation distance, so the slow detector response does not prevent resolving fringes.

4. Electric Probe Measurements.

The electron density associated with the gun produced plasma was determined on the test stand apparatus[6] using a double floating electric probe.[11] By varying the voltage between the probe electrodes on a shot-to-shot basis, an I-V characteristic for the probe at any time during the plasma discharge could be generated. The plasma temperature can be determined from the shape of the I-V characteristic.[11] Assuming the probe areas are equal the net current measured in the probe circuit, I_p, is given by[11]

$$I_p = I_i \tanh(eV/2kT_e). \qquad (7)$$

Here, I_i is the ion saturation current (obtained from the probe characteristic), V is the applied voltage between the probes, and k is Boltzmann's constant. Equation (7) is used to calculate T_e.

The electron density is related to I_i through

$$I_i = \langle Z \rangle en_i \langle v \rangle A = en_e \langle v \rangle A, \qquad (8)$$

where e is the electron charge, A is the probe collection area, and $\langle v \rangle$ is the ion collection velocity appropriately averaged over the probe surface. Two limiting cases are: 1) high velocity, directed plasma flow, which applies at early times in the gun discharge and 2) a quiescent, thermal plasma. If the plasma flow speed $v_D \gg c_s$, where c_s is the ion sound speed = $\sqrt{kT_e/M_i}$ (M_i is the ion mass), Eq. (8) results in[12]

$$n_e = \frac{1}{2rl}\left(\frac{I_i}{ev_d}\right) \quad (v_D >> c_S) \; . \tag{9}$$

Here r and l are the probe radius and length, respectively. Typically $r \simeq 0.025 - 0.05$ cm and $l \simeq 0.5$ cm. For the thermal plasma case, $\langle v \rangle \simeq c_s$ and use of Eq. (8) results in[11]

$$n_e = \left(\frac{1.64}{Ae}\right) \frac{I_i}{\sqrt{kT_e/m_i}} \quad (v_D \leq c_S) \; . \tag{10}$$

where the dimensionless factor 1.64 is a geometrical correction. Because of uncertainties in the value of $\langle v \rangle$ and A, the value of n_e determined by Eqs. (9) and (10) can be uncertain by a factor $\simeq 2$.

Measurements were made on the test stand apparatus with a probe and biased Faraday cup 10 cm from the gun and no screen present. Typical results are shown in Fig. 12. The gun current is an underdamped sinusoid with a peak value of 35 kA and .5 μs quarter period. The Faraday cup and double electric probe are biased to collect ion saturation current. Both probes peak at the same time, t = 1.6 μs. At later times, the electric probe has a large signal while the Faraday cup signal drops to zero. This is attributed to a decrease in plasma flow velocity, making the Faraday cup insensitive to the ambient plasma density which is recorded by the electric probe. The microwave transmission measurements, described in the previous section, indicate cutoff ($n_e > 6 \times 10^{13}$ cm^{-3}) at $\simeq 2.5$ μs, as indicated in Fig. 12. The data indicate that at $t \simeq 1.6$ μs, $n_i \simeq 1.5 \times 10^{13}$ cm^{-3} (Eq. (9)) with $v_D \simeq 6 \times 10^6$ cm/sec. These data are supported by the spectroscopic and microwave transmission measurements. The temperature is $T_e \simeq 6$ eV. Later in time, the density increases to $> 10^{14}$ cm^{-3}.

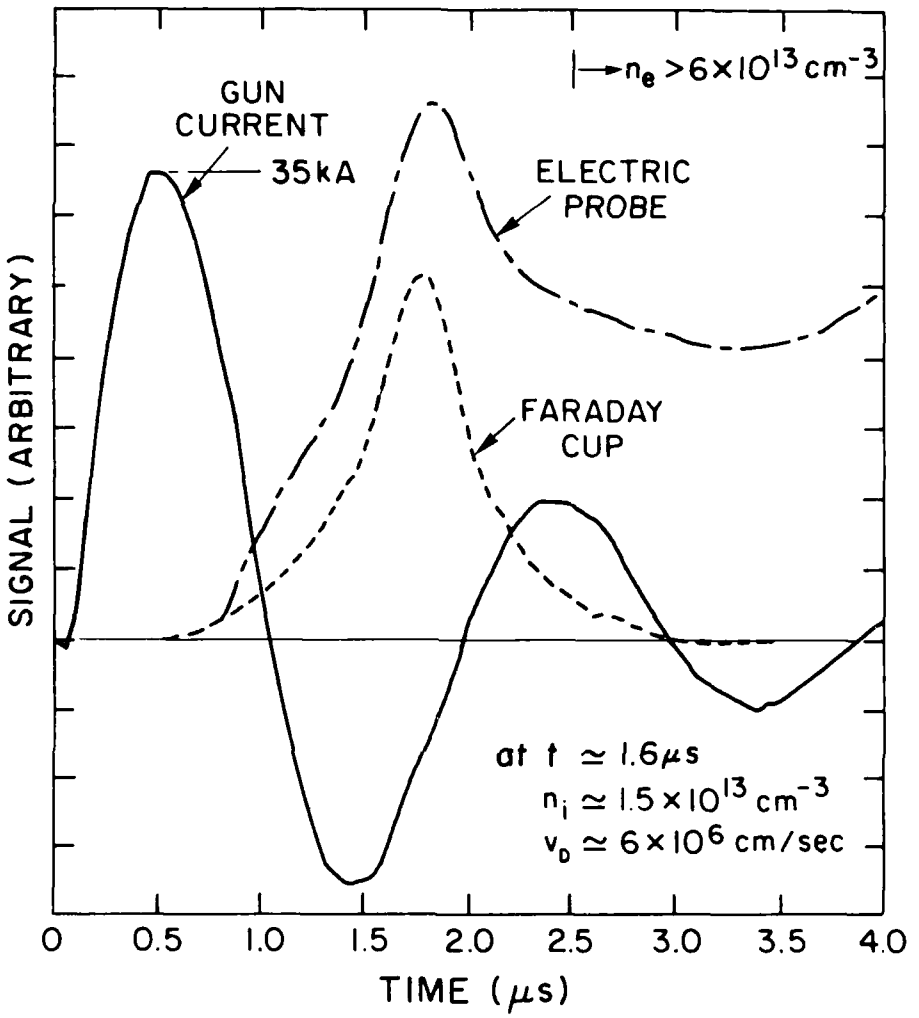

Fig. 12 Typical data from double floating electric probe and Faraday cup located 10 cm from a plasma gun. Also shown is the gun current.

B. In Situ Measurements.

Results from in situ electric probe measurements[6] are displayed in Fig. 13. The in situ measurements were made inside Gamble I without firing the generator, to characterize the plasma conditions at the time when the PEOS begins to carry current in the presence of electrodes. The switch region was ≃ 6 cm in length and z=0 defines the geometrical location of the generator end of the switch. On an actual Gamble I shot, the load would be at z ≃ 24 cm. Three guns were used, placed 10 cm from the cathode and 120° apart. For all data shown in Fig. 13, $T_e \simeq 7$ eV. In the left hand portion of Fig. 13 the axial variation of n_e at t ≃ 1.8 μs (approximately the time of peak Faraday cup signal) is shown. This is the time that would result in optimum switching for Gamble I. The measurements were made midway between the center conductor and outer conductor, under the position of one gun. As seen from the figure, the density maximum is $n_e \simeq 6 \times 10^{13}$ cm^{-3} in the middle of the switch region and falls off toward the load and generator ends. The azimuthal variation, shown in the right hand portion of Fig. 13, was obtained in the midplane of the switch region (z = 3 cm) and radially midway between the inner and outer conductors. The data were not as reproducible in this measurement in comparison with the reproducibility of the axial measurements, but they are quite acceptable. Again, these data are taken at t ≃ 1.8 μs. To within ≃ ± 35% the density is uniform azimuthally with $n_e \simeq 4.5 \times 10^{13}$ cm^{-3} and some suggestion of peaking near the gun locations. Thus, for times of interest (t < 2 μs), the plasma density and temperature in the inter-electrode region are essentially the same as those associated with the gun generated plasma when no surfaces are present. These results are supported by the spectroscopic and photographic

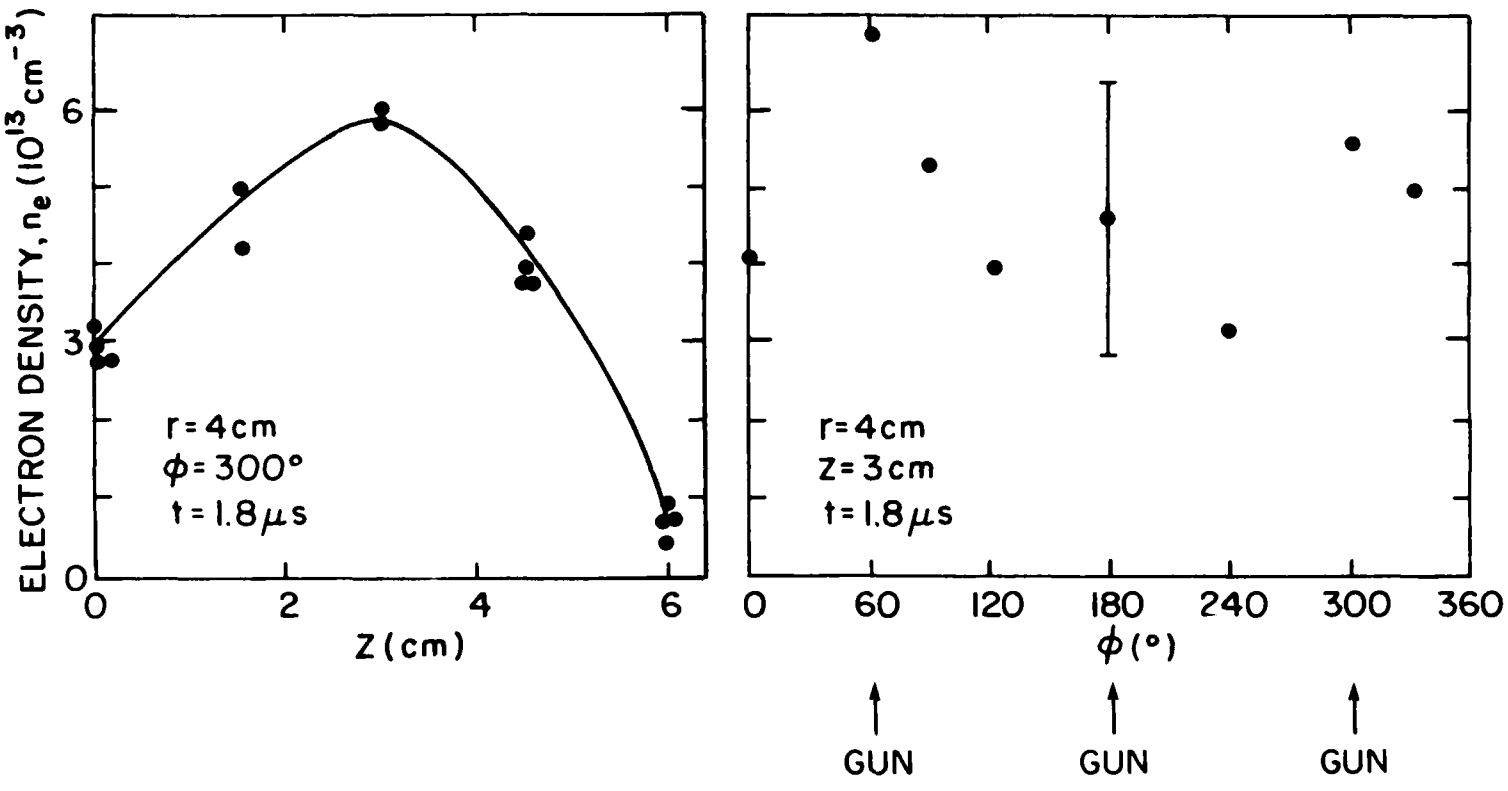

Fig. 13 Electron density distribution in the axial and azimuthal directions at t = 1.8 μs, determined from double floating electric probe.

data taken on the test stand. The density continues to rise to 3×10^{14} cm^{-3} at $t = 6$ μs. Another important point is that the degree of uniformity illustrated in Fig. 13 using the Gamble I geometry and three plasma guns is apparently sufficient to observe good switch behavior.

The data presented in Sec. II give a consistent picture of the carbon gun plasma parameters. The plasma is primarily doubly ionized carbon, $\langle Z \rangle \simeq 2$, with an electron temperature of $T_e \simeq 6 - 8$ eV. The electron density increases in time and reaches $\simeq 6 \times 10^{13}$ cm^{-3}, 10 cm from the source, at $t \simeq 2.5$ μs. The plasma flow velocity is 5 - 10 cm/μs, higher than the ion sound speed $c_s \simeq 1$ cm/μs. For $t < 2$ μs, the bulk of the inter-electrode plasma is unaffected by the presence of the metal electrode surfaces. The density between the surfaces continues to increase and temperature decreases with time to $n_e \simeq 3 \times 10^{14}$ cm^{-3} and $T_e \simeq$ eV at $t \geq 6$ μs. Lower charge state carbon (CI and CII) and hydrogen evolve from the electrode surfaces $\simeq 1.5$ μs after the source is fired and begin to slowly diffuse into the inter-electrode region at $\simeq 1$ cm/μs. These measurements give the approximate values that have been used by NRL in successfully modeling the PEOS.

The flashboard sources have not been as extensively diagnosed as the plasma guns. The approximate values of the plasma perameters are expected to be the same, based on observed switch performance.

III. CONDUCTION PHASE CHARACTERIZATION

A. Time Resolved Photography.

A sequence of streak camera photographs taken of the switch region during Gamble I PEOS experiments[5] is shown in Fig. 14. The load was a short circuit. Three equally spaced plasma guns were located 10 cm from the 2.5-cm radius cathode. Here, time is measured from the initiation of the generator current. Four photographs are shown with the associated current waveforms. Each photograph corresponds to a specific time delay, τ_D, between firing the plasma guns and the initiation of current flow through the switch. At τ_D = 1.3 μs, no current is carried by the switch and the only visible light is that from the gun region. For the next photograph τ_D = 1.9 μs, which is near the optimal delay for switching purposes. As current flows through the switch the outer, screen electrode (anode) becomes bright first, followed by a less intense emission from the inner-electrode (cathode). The region between electrodes does not become bright and the discharge is apparently diffuse. For τ_D = 2.8 μs, the switching action is sluggish. More current is carried by the switch for a longer time and both electrodes are bright, the anode lighting up first. The inter-electrode region is still diffuse. When τ_D = 4.5 μs, the switch conducts all the current and the inter-electrode region becomes very bright, probably indicating an arc. This may be a result of the plasma associated with surface interactions as discussed in Sec. II. Intense light from the electrodes or switch region is not observed in the absence of switch current. This indicates that there is an interaction at the electrodes during the conduction phase. The emitted light appearing on the anode side

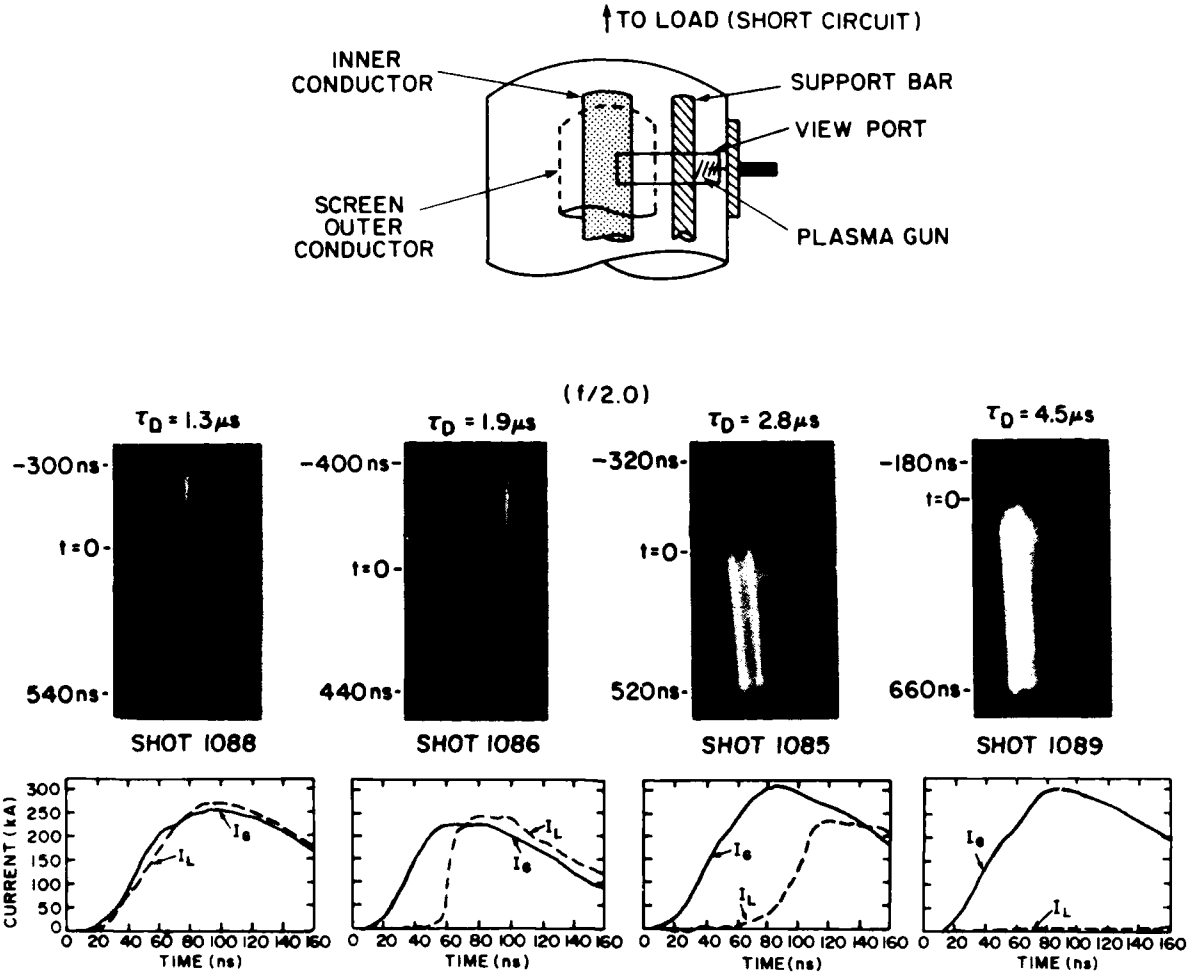

Fig. 14 Upper: Arrangement for streak camera photography during a shot on Gamble I. Middle, lower: Four streak photographs and current traces for various generator delay times.

first may be a result of the anode being a semi-transparent screen. The cathode is solid aluminum, so, in contrast with the screen, light emitted from the far side of the cylinder is not included in the line of sight. At this exposure level, light emitted from the inner and outer conductors as a result of the initial injected plasma (Figs. 2 and 3) is not visible. Thus, the emitted light in these regions are associated with the switch carrying current. This strongly suggests that electrons are emitted from the entire cathode surface.

The same optical arrangement of Fig. 14 was employed with a faster sweep for the streak camera. The result is illustrated in Fig. 15. Here again the light from the anode surface appears first at $t \simeq 60$ ns. Note that this light appears after the conduction phase, as seen from the current trace in the lower portion of the figure. This may be a result of the finite time for atomic excitation, an indication that the plasma density within several millimeters of the cathode is not high enough during conduction for strong light emission to occur. Using approximate relations for collisional excitation rates,[7] one can very crudely estimate that to see light emission resulting from collisional excitation during conduction ($\lesssim 100$ ns), $n_e > 10^{15}$ cm^{-3} is required near the surface. We conjecture from the spectroscopic results (Sec II.A.2) that before conduction begins, 0.2 cm from the surfaces, $n_e \sim 10^{14}$ cm^{-3}.

Shown in Fig. 16 is a somewhat different optical arrangement used on the Pollux device by the group at Karlsruhe to observe light emission along a portion of the PEOS cathode.[13] The light emission begins on the generator side of the PEOS and proceeds to the load side at a speed of

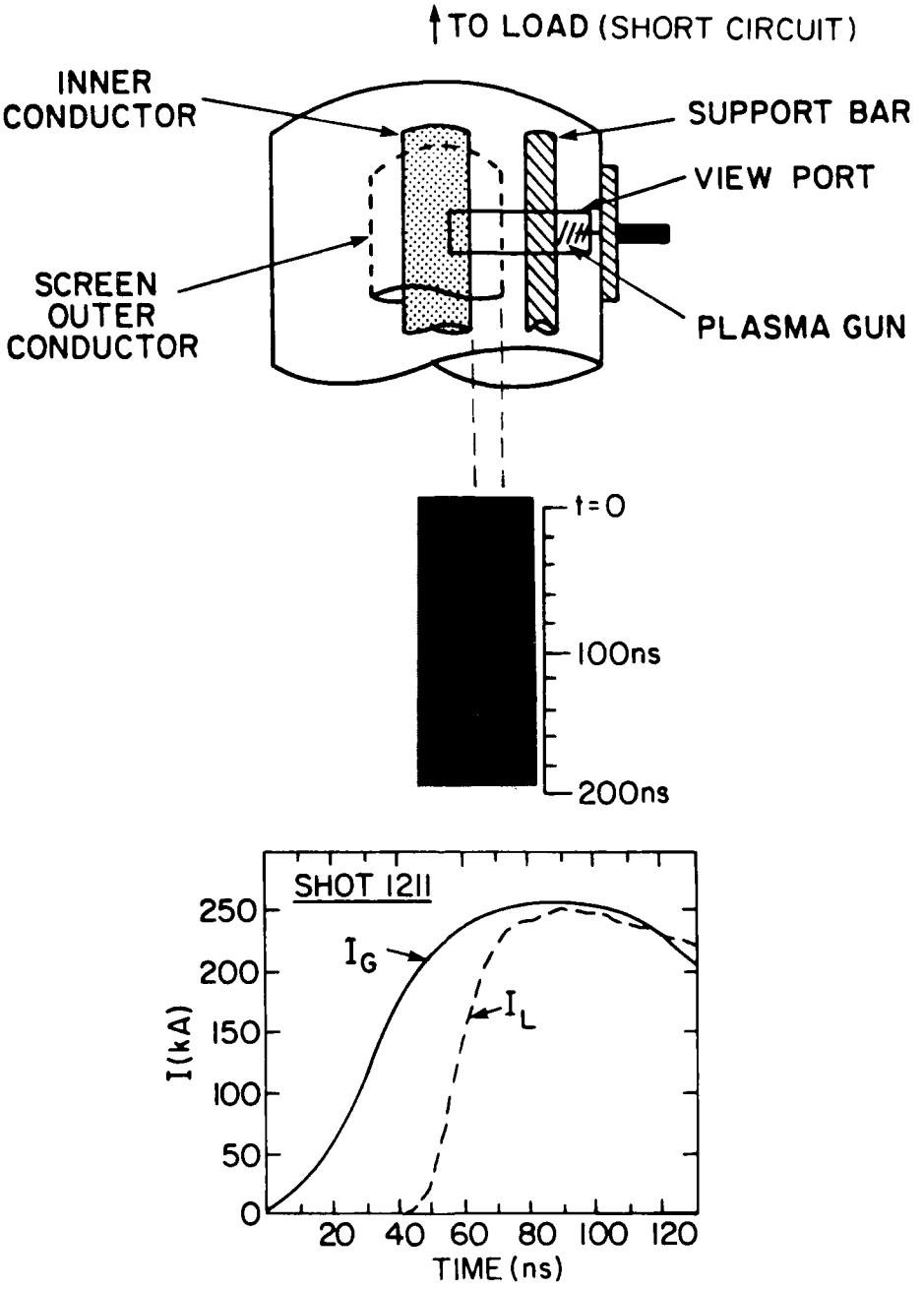

Fig. 15 Upper: Arrangement for fast streak camera photography during a shot on Gamble II. Middle, lower: Fast streak photograph and current trace.

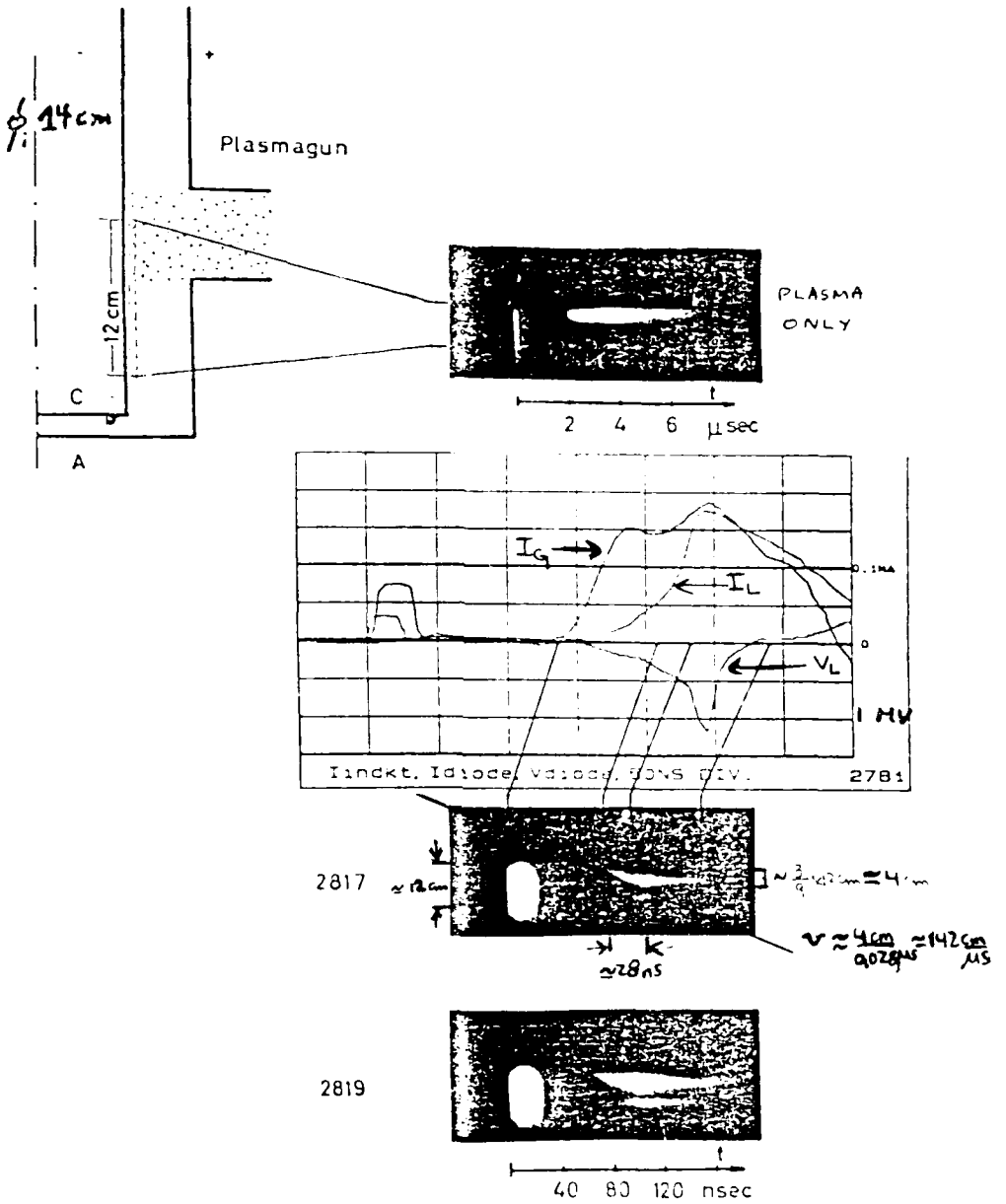

Fig. 16 Upper: Arrangement for fast streak camera photography during a shot on Pollux. Middle, lower: Current traces and fast streak photographs. (Data from Ref. 13).

≃ 150 cm/μs. The Karlsruhe group suggests[13] that the interpretation of these photographic data supports the previously proposed NRL current controlled conduction phase model.[1,14.15] If the magnetic field penetration is slow compared with the current rise the critical current density for erosion is exceeded locally, before the current is carried throughout the full axial extent of the switch plasma. In this case the erosion front migrates through the switch plasma. The conduction time is determined by the speed of this erosion front and the axial extent of the plasma. As soon as the erosion front reaches the load end of the switch plasma, the switch begins to open. This interpretation agrees with the conduction current measurements and magnetic probe data presented in the next section.

B. Conduction Current Scaling

A fundamental aspect of the NRL current controlled PEOS model [1,14,15] is the assertion that the switch conducts with no voltage appearing at the load end of the switch up to a current limit that is specified by the injected plasma conditions as follows:

$$I_s^o \simeq I_e^o = \left(\frac{m_i}{Zm_e}\right)^{1/2} Ze\left(n_i\langle v\rangle\right)2\pi r_c l_o \ . \qquad (11)$$

This current limit is derived from the Child-Langmuir, non-relativistic, bipolar, space-charge-limited flow condition in cylindrical geometry. Here $I_s^o(I_e^o)$ is the peak switch (electron) current, m_e is the electron mass, r_c is the PEOS cathode radius, l_o is the initial switch length, and $\langle v\rangle$ the average radial component of the ion velocity at the cathode surface. The term in brackets, $n_i\langle v\rangle$, is the ion flux density at the cathode associated with the

injected plasma. We have assumed for this work that the effect of axial $\bar{J} \times \bar{B}$ forces can be neglected. This assumption is supported by experiments in which the PEOS has successfully opened (albeit more slowly than for short conduction time experiments) after conducting for several hundred nanoseconds (see Ref. 14 and Sec. III.B.4 below).

1. Scaling of I_s^o of with τ_D ($n_i\langle v\rangle$).

According to Eq. (11), $I_s^o \propto n_i\langle v\rangle$. The quantity $n_i\langle v\rangle$ is extremely difficult to measure. Measurements of n_i alone (in the bulk of the plasma) using spectroscopy, microwave transmission, and double floating electric probes are described in Sec II. Usually one uses for $\langle v\rangle$ the injected plasma drift speed v_d. At best, this is an overestimate of $\langle v\rangle$. One control over $n_i\langle v\rangle$ the experimentalist has is the relative generator-to-gun delay time, τ_D. The measurements (including Faraday cups[5,6]) all suggest that with delays of interest for fast switching ($\tau_D < 2.2$ μs), as τ_D increases n_i also increases. If one assumes that $\langle v\rangle$ scales as the time of flight ($1/\tau_D$), then n_i increases fast enough that $n_i\langle v\rangle$ also increases as τ_D increases (as is supported by the usual interpretation of the Faraday cup signal, at least until it peaks). Thus, by varying τ_D the measured peak switch current can be used in conjunction with Eq. (11) and the estimates of $n_i\langle v\rangle$ in a simple, self-consistency check. This by no means constitutes a measurement of $n_i\langle v\rangle$ and only supports the scaling of I_s^o with $n_i\langle v\rangle$ in an approximate way.

Using Gamble I with a short circuit load, I_s^o was measured as a function of τ_D.[5] This was accomplished by simply taking the difference between the measured generator and load currents for shots with various τ_D. The ion density and drift velocity at different τ_D were estimated as described

above from double floating probes and Faraday cups and used in Eq. (11) to predict I_s^o. Results of these measurements are displayed in Fig. 17. The model and experimental results agree. Note that the values for n_i and $\langle v \rangle$ used in this analysis were not measured at the gap-plasma boundary, but represent our best estimate of those parameters in the bulk of the plasma.

2. Scaling of I_s^o with n_i.

The effect on I_s^o of varying only the density was investigated by adding more plasma guns and using the same τ_D. Results from Gamble I where I_s^o was measured as a function of τ_D with 3 and 6 guns are displayed in Fig. 18. Doubling the number of guns and firing at the same τ_D presumably increases n_i by a factor ~ 2 and, from Eq. (11), should roughly double I_s^o. The data indicate that within the scatter I_s^o increases by a factor $\simeq 1.5$, about 25% less than predicted. This descrepancy must be investigated further. Note that simply doubling the number of sources may not double the effective density. The scatter in I_s^o for a given arrangement of guns at any one τ_D is $\leq \pm$ 5% (Fig. 18). The scatter is more typically $\leq \pm$ 10% over all our experience on Gamble I, Gamble II, and Blackjack 5 with guns and flashboards. Data with six guns are also shown with a smaller storage inductance (115 nH vs. 185 nH). This was done to access higher current levels.

3. Scaling of I_s^o with r_c.

Using Gamble I with a short circuit load and three guns, the effect of varying the cathode radius on I_s^o was investigated.[6] Three different cathode radii were used; r_c = 2.5, 1.25, and 0.63 cm. In each

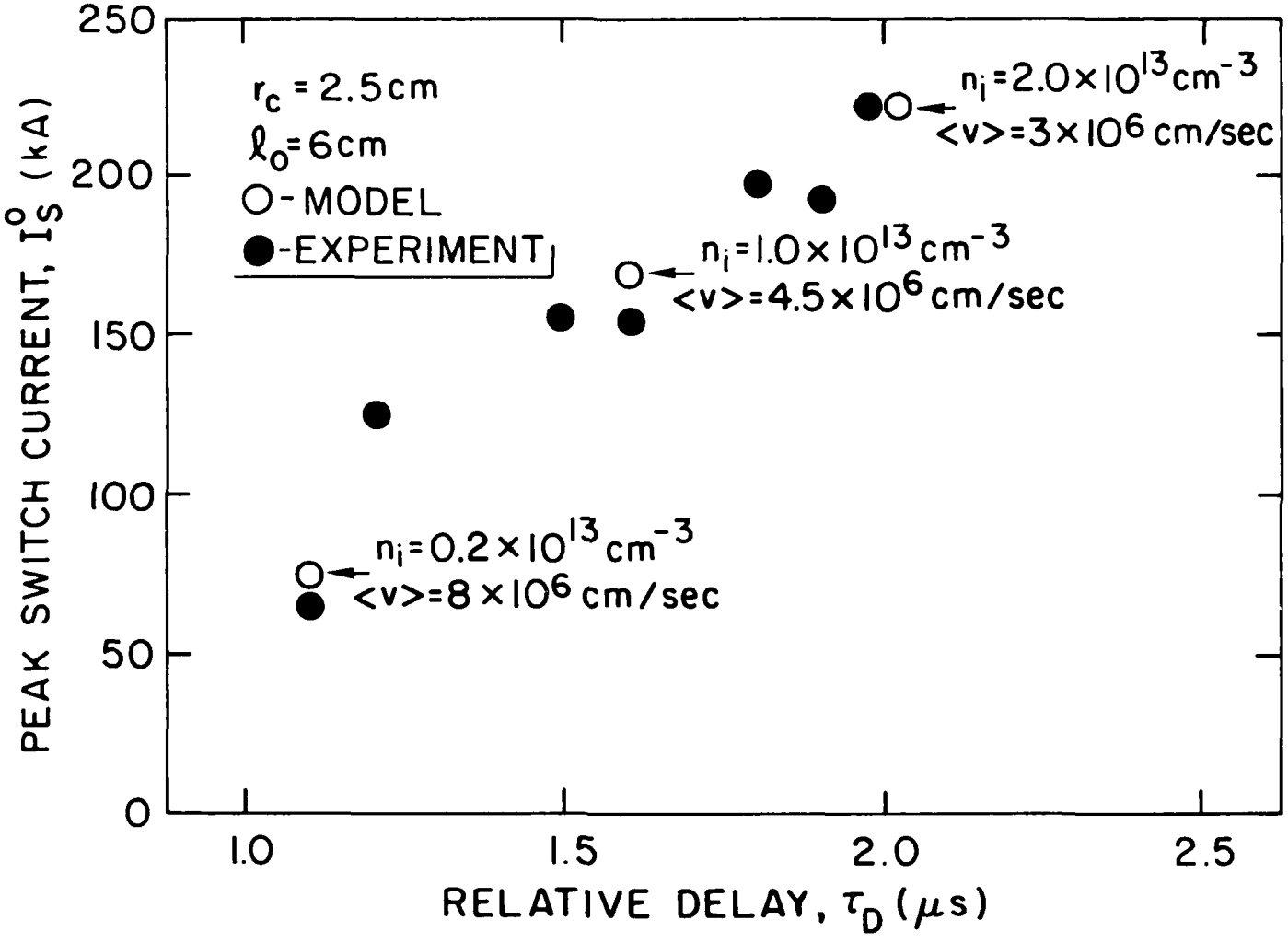

Fig. 17 Peak switch current, I_s^o, as a function of delay time, τ_D. Also shown is result of calculation using best estimate of $n_i\langle v\rangle$.

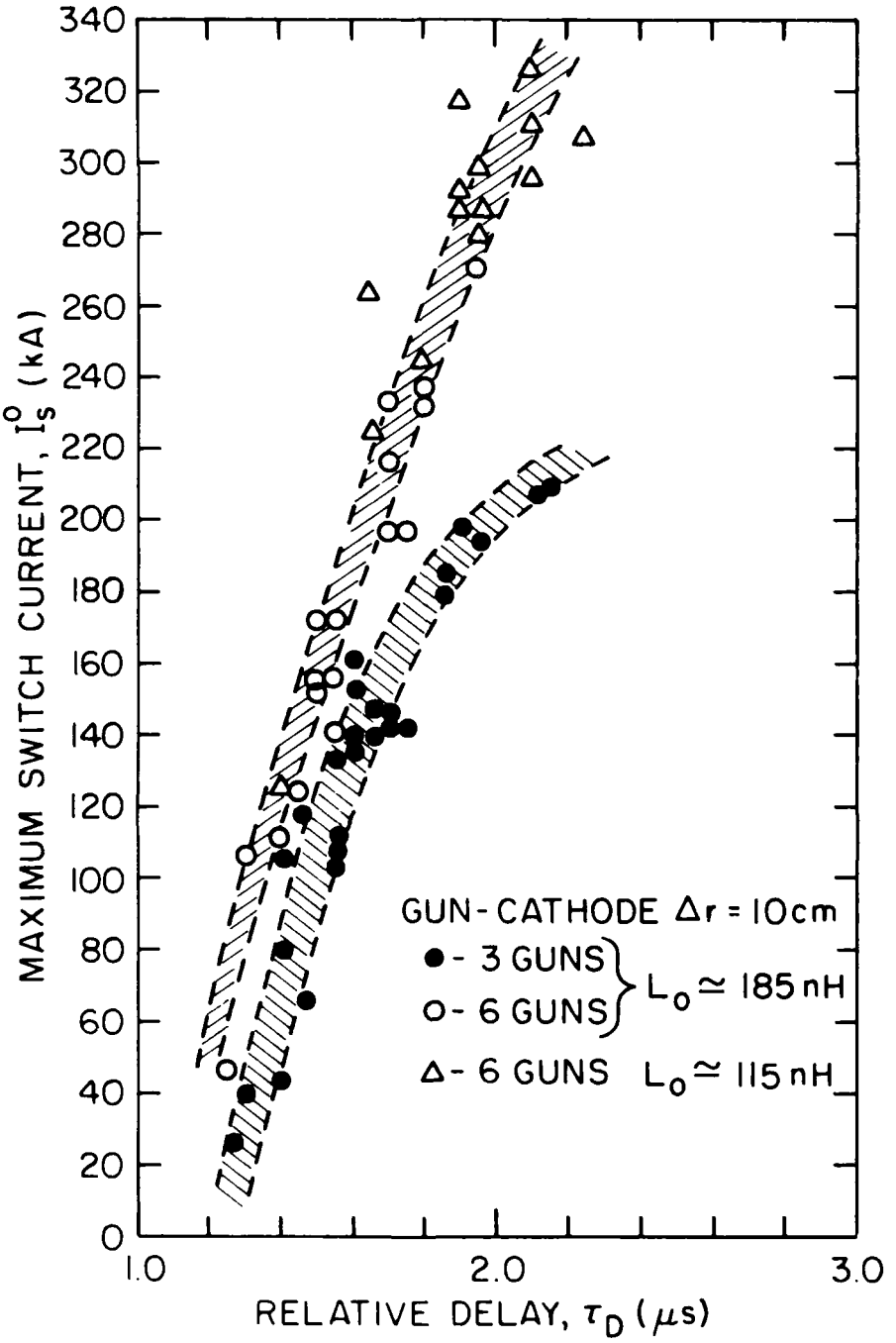

Fig. 18 Peak switch current, I_s^o, as a function of delay time, τ_D, for 3 and 6 guns. Also shown are data with 6 guns and reduced storage inductance.

case the gun-cathode distance was fixed at 10 cm, the switch AK gap was fixed at 2.5 cm, and three guns were used with $\tau_D \simeq 1.6$ μs. The results are plotted in Fig. 19. Also shown are the calculated I_s^o using Eq. 11. The calculation was normalized at $r_c = 1.25$ cm. Also, n_i was scaled with r_c ($n_i \propto 1/r_c$) to account for a density variation resulting from the change in volume of the switch region. The measurement and calculation agree over this limited range of data.

4. Scaling of I_s^o with Constant $n_i l_o$.

A third switch conduction scaling experiment was performed on Gamble I, in which the product $n_i l_o$, was held constant while n_i and l_o were each varied.[16] This was accomplished as illustrated in Fig. 20 by using the same 12 plasma guns distributed uniformly over 10-, 20-, and 30-cm lengths. When l_o was increased, the axial density of plasma sources was decreased by the same factor. The distance between the guns to the PEOS cathode was increased to 15 cm (the usual case being 10 cm) and $r_c = 2.5$ cm. The results are plotted in Fig. 21. Within the scatter ($\simeq \pm$ 25kA), I_s^o is independent of l_o for a given τ_D when the product $n_i l_o$ is held constant, in agreement with Eq. (11). Also plotted in Fig. 20 are data from the recent POP experiment.[14] Here a capacitor bank directly drives the identical Gamble I hardware used to obtain the other data in the figure at about half the current but for a factor of $\simeq$ 10 longer time. For up to $\simeq$ 100 kA, the scaling of Eq. (11) holds at a factor 10 longer conduction time, demonstrating the current controlled nature of the PEOS conduction. Above 100 kA other factors, such as the capacitor bank being drained of charge, the time variation of the plasma flux density at the cathode, and modification to the bipolar flow condition (not discussed here), may be important.

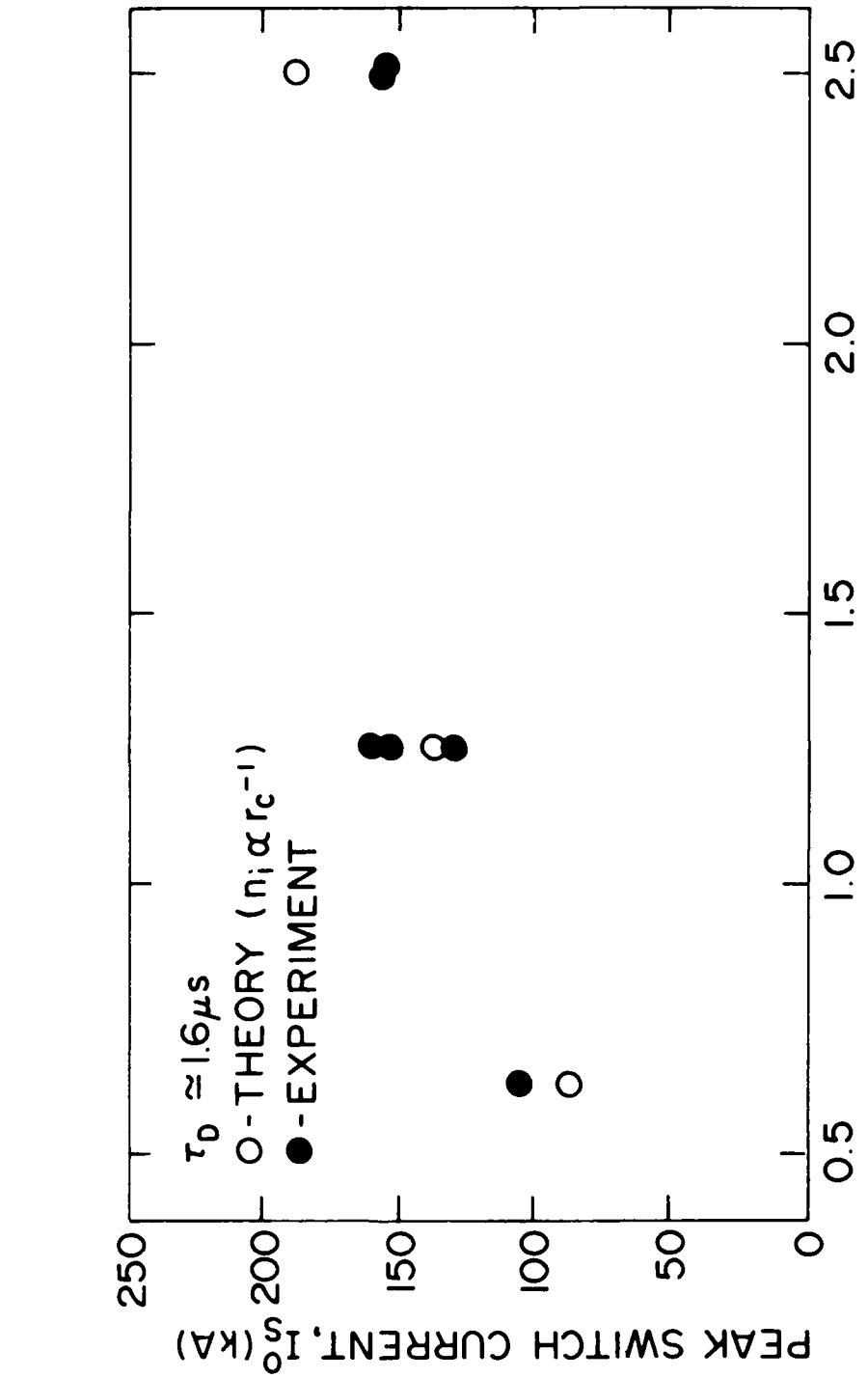

Fig. 19 Peak switch current, I_S^o, as a function of cathode radius, r_c. Also shown is result of calculation. For calculation, density was scaled with r_c to account for volume change.

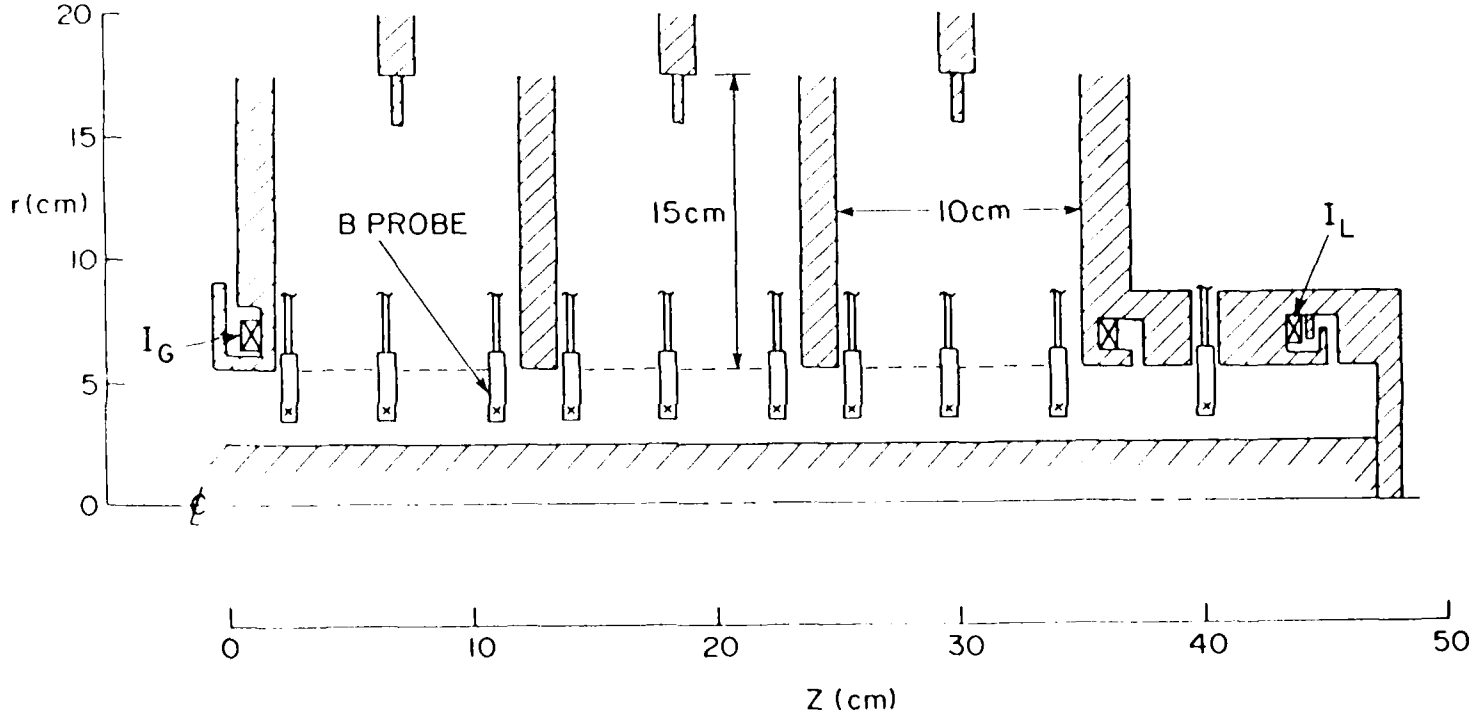

Fig. 20 Schematic of setup on Gamble I for varying n_i and l_o while keeping $n_i l_o$ constant. Also shown are locations for magnetic probes.

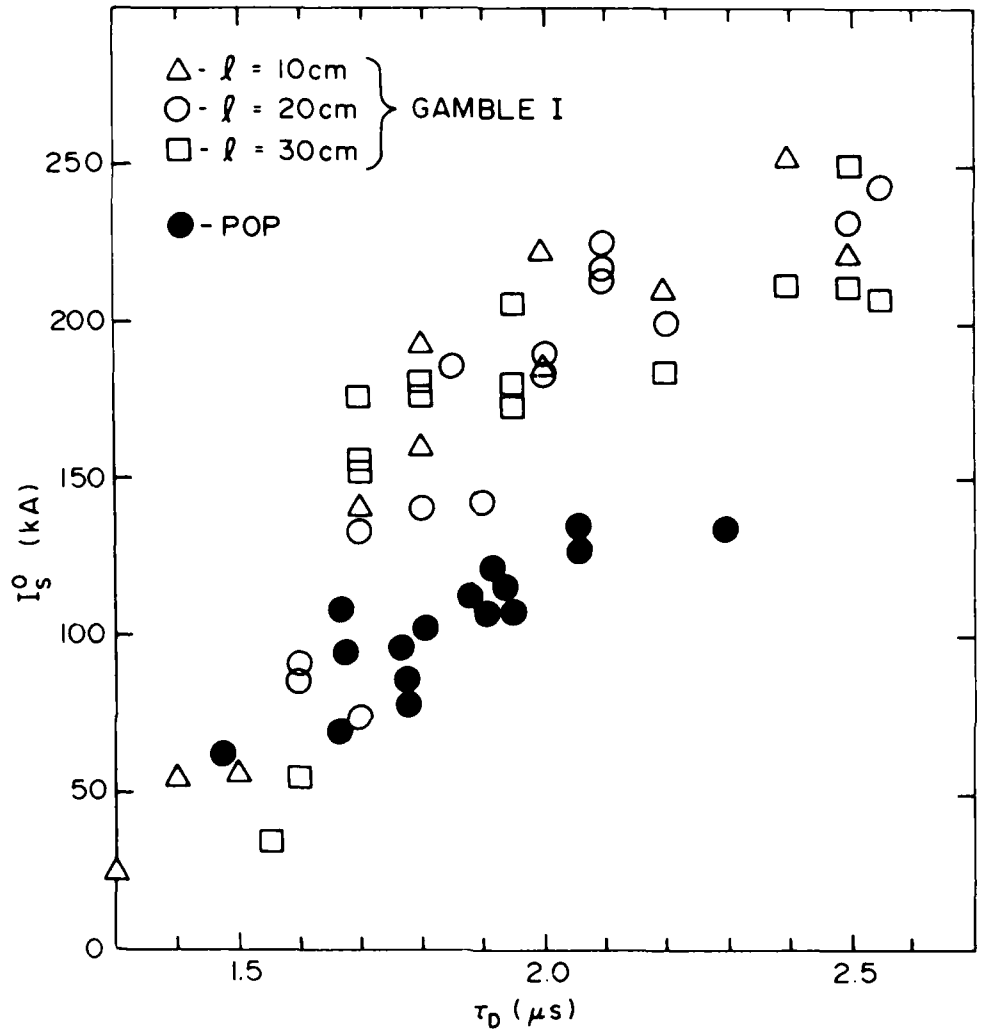

Fig. 21 Peak switch current, I_s^o, as a function of relative delay time, τ_D, for 10-20-, and 30-cm long switch where $n_i l_o$ was constant for each τ_D. Also shown are results with the same $n_i l_o$ but a factor 10 longer conduction time (POP).

To summarize Sec III.B, the peak current conducted by the PEOS scales approximately in accordance with Eq. (11). The estimates for the values of the plasma parameters obtained from the measurements described in Sec. II and the measured peak switch current are consistent with Eq. (11). The conduction phase of the PEOS appears, from the external current measurements, to be current controlled. Internal measurements of the magnetic field, discussed in what follows, support this assertion and reveal the details of the current distribution in the PEOS.

C. Magnetic Field Measurements.

A schematic of the setup for measuring the magnetic field in the PEOS[15] during conduction and opening is given in Fig. 22. Five small probes measure the local magnetic field in the PEOS plasma during fast opening shots. The dots represent typical measurement locations. The probes are potted inside 5-mm diam quartz tubes, inserted into the switching region through the screen anode, and oriented to measure the azimuthal field, $B_\theta(t)$. Usually five axial locations (z) at a common radius (r) were sampled on a single shot. The probes are calibrated on shots with no plasma relative to the Rogowski loops that measure the generator (I_G) and load (I_L) current. Several experimental checks were made to determine the perturbative influence of the probes on the measurement. The presence of the probes does not affect the measured currents I_G and I_L and the signal obtained from any probe in a given position is independent of the location of other probes. The plasma energy loading on the probes is too small to ablate significant material from the quartz during the time of interest, as evidenced by the condition of the

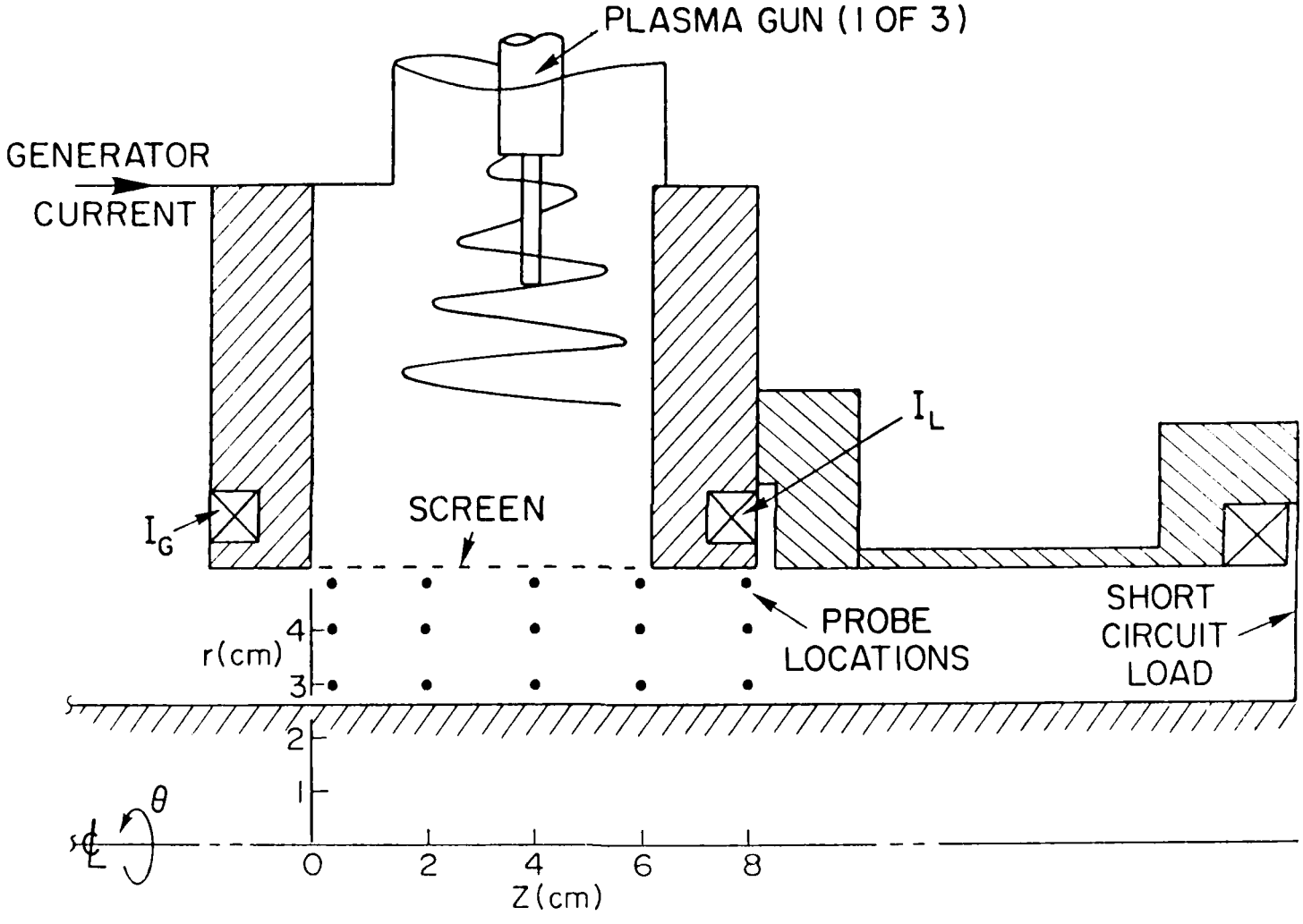

Fig. 22 Schematic of setup for magnetic probe measurements.

probes after use and as supported by analytical estimates. The probe signal goes to zero when it is placed outside the screen. Finally, the probes have a sub-nanosecond response time.

In Fig. 23(a), the probe signals for a fast opening shot are plotted in units of current for various axial positions at the same r.[6] Also plotted is I_L. If the field is azimuthally symmetric, then the magnetic field, B_θ, measured by the probe is related to the current, I, flowing under the probe through a circle of radius r by

$$I(A) = B_\theta\,(G) \times 5r(cm), \tag{12}$$

where r is the probe radial position. In this case the difference between the signal seen by two probes at the same r but different z is associated with the current flowing under one probe but over the other and thus having a radial component to its flow. As seen in the figure, the current steadily penetrates into the switch plasma with switch opening beginning when the current reaches the load end of the plasma.

To check the assumption of azimuthal symmetry, the probes were arrayed azimuthally at the same r and z. Data for the case[6] of a fast opening shot are shown in Fig. 23(b). To within measurement accuracy, the signals indicate an azimuthally symmetric discharge verifying the use of Eq. (12).

These results (for fast opening) are contrasted with a shot at a longer τ_D where a slow opening was observed[6] in Fig. 24. As shown in

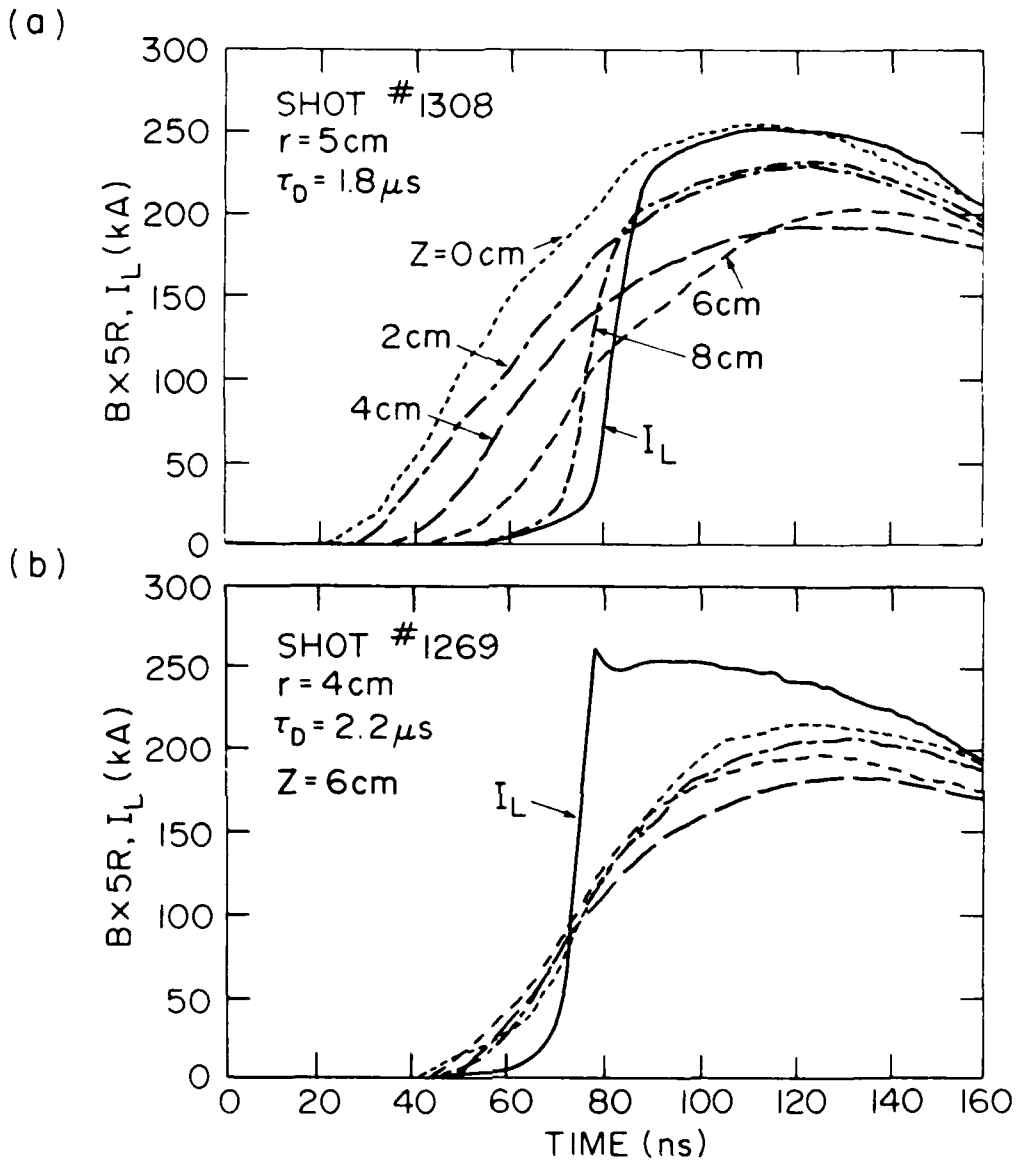

Fig. 23 (a) Magnetic probe signals, in units of current, as a function of time at five axial positions for a fast opening shot. (b) Magnetic probe signals, in units of current, as a function of time at four azimuthal positions for a fast opening shot.

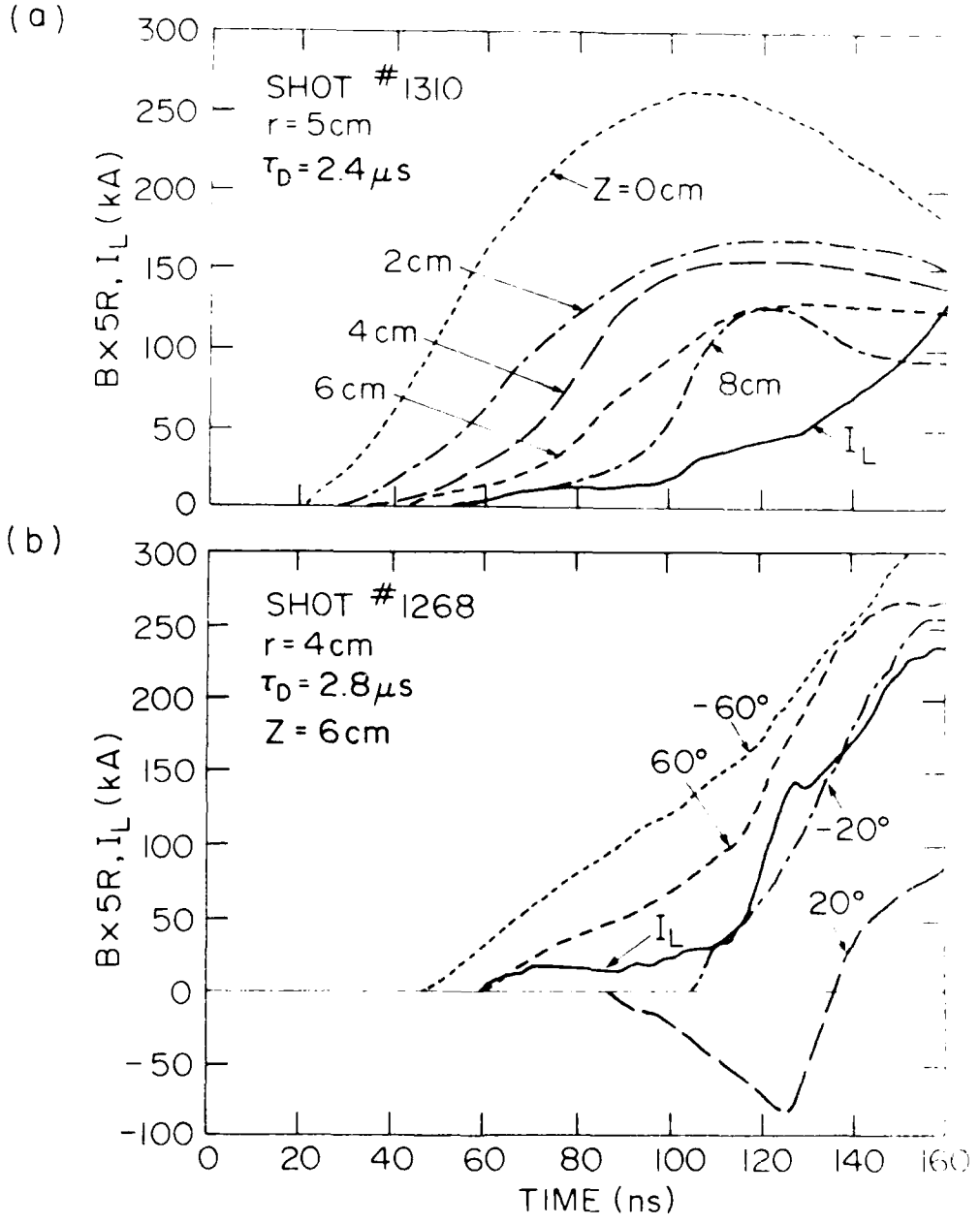

Fig. 24 (a,b) Same as Fig. 21(a,b), except for a slow opening [illegible].

Fig. 24(a), the current still penetrates along z. However, as shown in Fig. 24(b), the discharge is clearly not azimuthally symmetric and interpretation of the probe signals as current according to Eq. (12) is incorrect. In this case, the discharge appears to be highly filamentary. Recall that the time resolved visible photography, described in the previous section, indicates the nature of the discharge is qualitatively different depending on value of τ_D (see Fig. 14). Also, the results of time resolved photographic, spectroscopic, microwave, and electric probe measurements described in Sec. II suggest that at large τ_D the switch plasma characteristics are significantly different (high density, low $\langle v \rangle$) from those at small τ_D.

The rate of penetration of magnetic field into the switch plasma was investigated[17] by using an axial array of 10 probes located radially midway between the PEOS anode and cathode in a 30-cm long switch as illustrated in Fig. 20. The long switch allows many probes to be used, improving spacial resolution. The axial position of the leading edge of the magnetic field (i.e., the first non-zero point of the traces in Fig. 23(a)) is plotted as a function of time for shots with different delay times in Fig. 25. Fast switching occurs for τ_D = 1.6 and 2.0 μs. For these delays the front speed, v_F, is fairly constant and very high, $\geq 10^3$ cm/μs. These observations argue against any mass motion associated with this front speed. As the time delay increases, v_F decreases. This is a result of the larger density associated with larger τ_D. At the largest τ_D, the front never reaches the load end of the switch and the switch does not open.

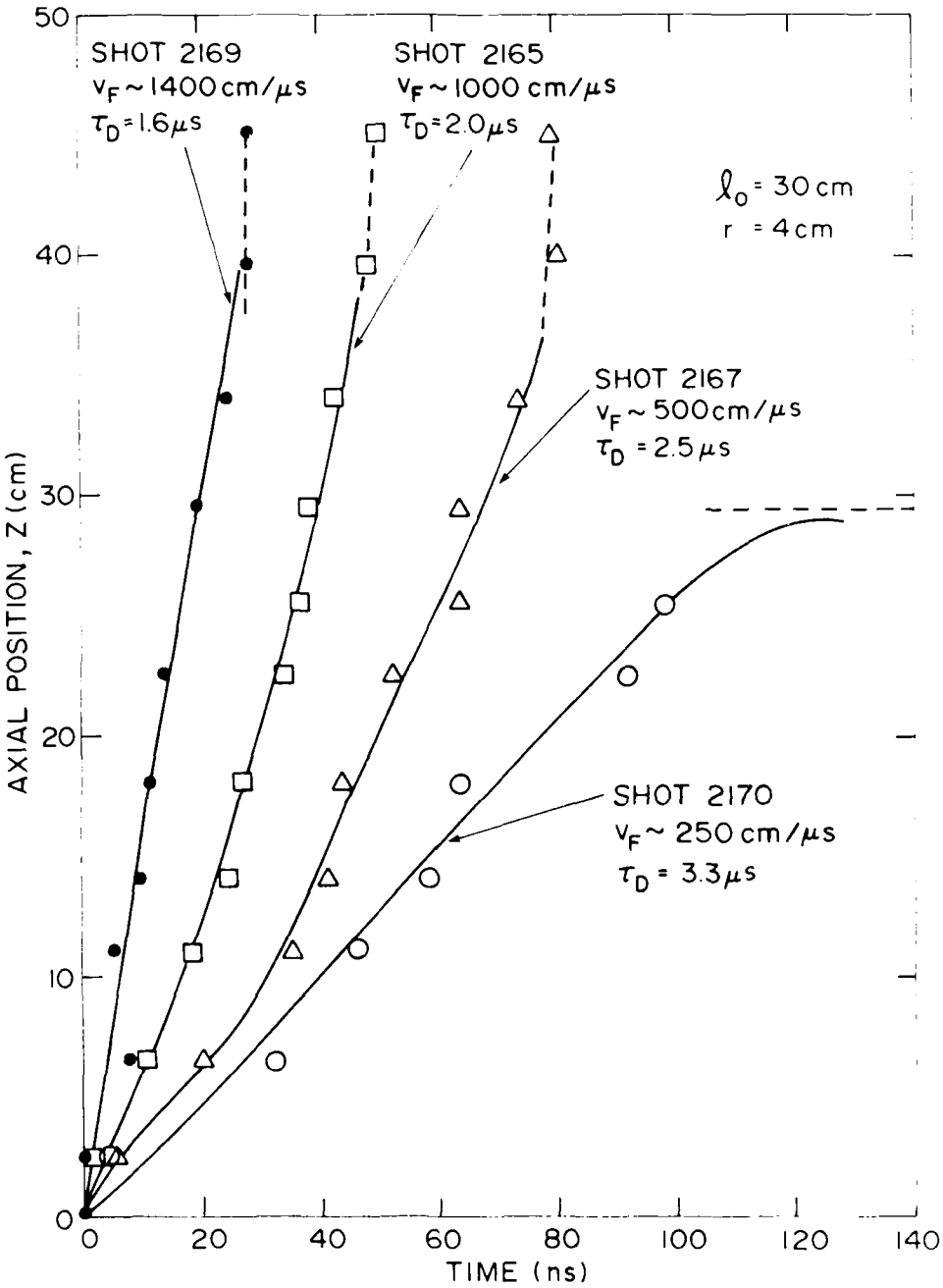

Fig. 25 The axial position of the leading edge of the magnetic field (current channel) front as a function of time for four time delays.

The distribution of current in the switch was characterized by plotting the probe signal as a function of axial position, z, at given times. These data are displayed for 10- and 30-cm long switches on Gamble I[17] in Figs. 26 and 27. When the initial switch length, l_o, was increased by a factor of by 3, the axial density of plasma sources was decreased by 3, so $n_i l_o$ was held constant as described previously. The probes were located radially midway between the switch anode and cathode. Because the current is azimuthally symmetric on fast opening shots (Fig. 23(b)), the probe signals are plotted in units of current, in accordance with Eq. (12). As per the previous discussion and the $\bar{\nabla} \times \bar{B}$ Maxwell equation, the axial derivative of the current distributions are proportional to the local radial current density. The data for the two cases look remarkably similar. The current is conducted over a fairly broad region, roughly half the original switch length in both cases. Note that the collisionless skin depth, c/ω_{pe}, where c is the speed of light and ω_{pe} the electron plasma frequency, is only a few millimeters for the injected plasma conditions. The current density remains nearly constant during the conduction phase, and the switch begins to open when the leading edge of the current channel reaches the load end of the switch plasma. These observations motivate the conduction phase portion of the current controlled PEOS model,[15] in which the switch current density remains approximately constant while the switch current increases during conduction, until the current channel can no longer broaden, i.e., a current limit is reached. They also give insight into the mechanisms responsible for the peak conduction current scaling results discussed previously in Sec. III.B.1.4 (Figs. 17-19 and Fig. 21).

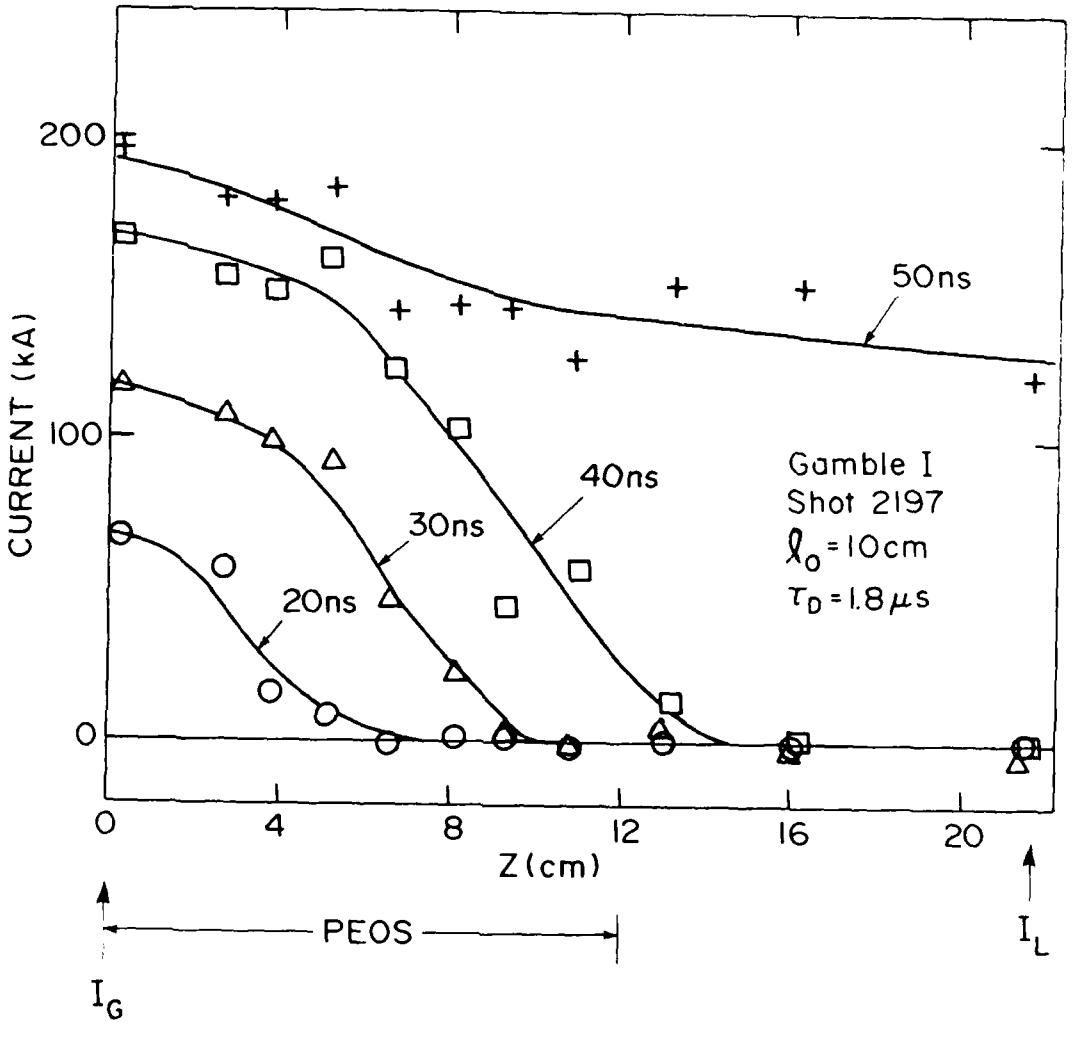

Fig. 26 Current distribution at various times in a 10-cm PEOS on Gamble I.

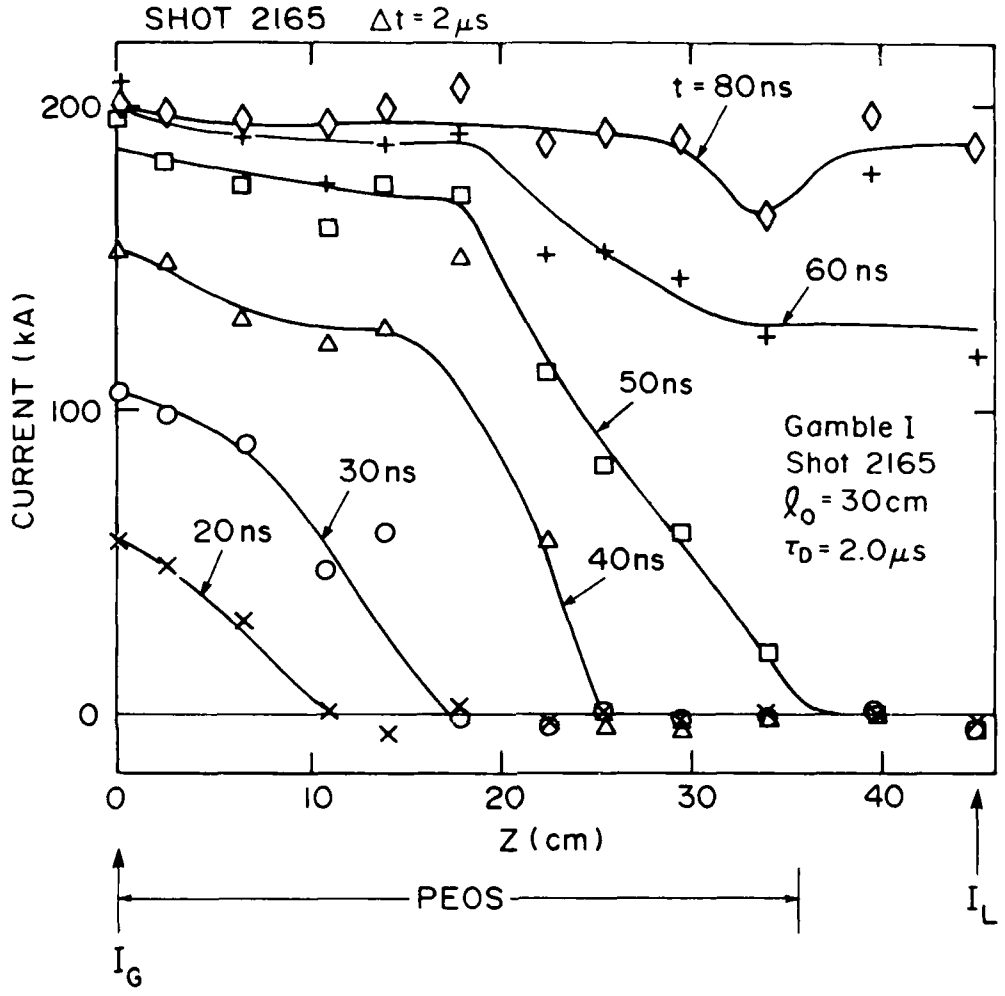

Fig. 27 Current distribution at various times in a 30-cm PEOS on Gamble I.

These results are also observed in the recent, previously described POP experiment,[14] as illustrated in Fig. 28. The data indicate the same broad current channel and constant, radial current density features of the Gamble I data shown in Figs. 26 and 27 (taken at one tenth the conduction time). The time delay in this case was smaller than in Figs. 26 and 27, so the switch opened at a lower value of current.

Direct verification of the radial nature of the current flow during conduction is provided by magnetic probes separated in radius by ~ 1 cm and placed at the same axial location during a shot.[6] Measurements over the entire switch region indicate that at a given z the magnetic field front arrives at all radii simultaneously as it moves steadily through the axial extent of the switch plasma.

Indirect support of the radial nature of the current flow and azimuthal symmetry during conduction comes from measurements with floating potential probes.[18] The probes were placed at the same axial position, but separated in radius and azimuth. The probe signals indicate the presence of high energy electrons. The signal arrival time was identical at the different radial and azimuthal positions. When the probes were placed at the different axial positions but at the same r, the signal arrival time tracked the magnetic field front speed, v_F (see Fig. 25).

An important point in discussing the conduction phase of the current controlled PEOS model is that the measurements made in the switch plasma are used to infer the magnetic field (current) penetration at the cathode.[15] Probes placed as close as 0.5 cm from the cathode show the same

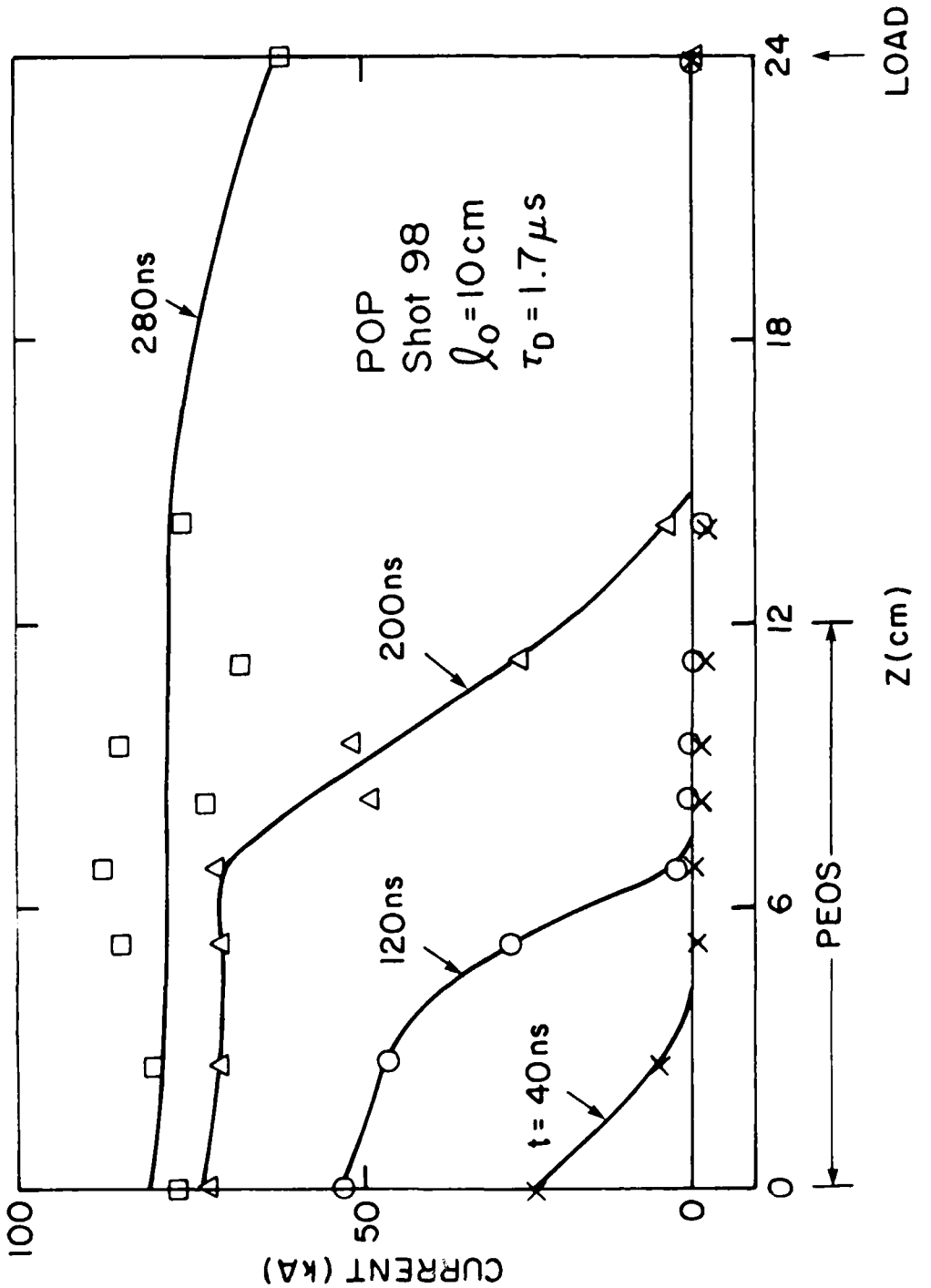

Fig. 28 Current distribution at various times in a 10-cm PEOS on POP.

behavior described above. Supportive data are provided by results from the recent (June 1986) Sandia National Laboratories/Naval Research Laboratory/Maxwell Laboratories, Inc. PEOS experiment on Blackjack 5 in support of PBFA II. Data from a surface magnetic probe placed in the switch cathode 2 cm from the load end of the 12 cm long switch are shown in Fig. 29.[19] The probe detected no current (magnetic field) for ≈ 65 ns, then current at the probe location was measured for 15 ns before it began flowing in the load. This result is supported by the streak photography done by the group at Karlsruhe[13] (see Fig. 16), which suggests current penetration along the cathode at rates similar to V_F.

To summarize Sec. III.C, for time delays where fast switching occurs ($\tau_D \leq 2.2$ μs) the switch current is azimuthally symmetric and flows radially in a broad ($>>c/\omega_{pe}$), current channel. The switch begins to open when the leading edge of the current channel reaches the load side of the switch plasma. For usual operating conditions both the magnitude and the constancy of the rate of current penetration is incompatible with associated mass motion.

IV. SUMMARY:

In this report, we have presented results of measurements that: (1) characterize the initial switch plasma, (2) identify the parameters influencing the peak conduction current, and (3) reveal the nature of the current conduction process.

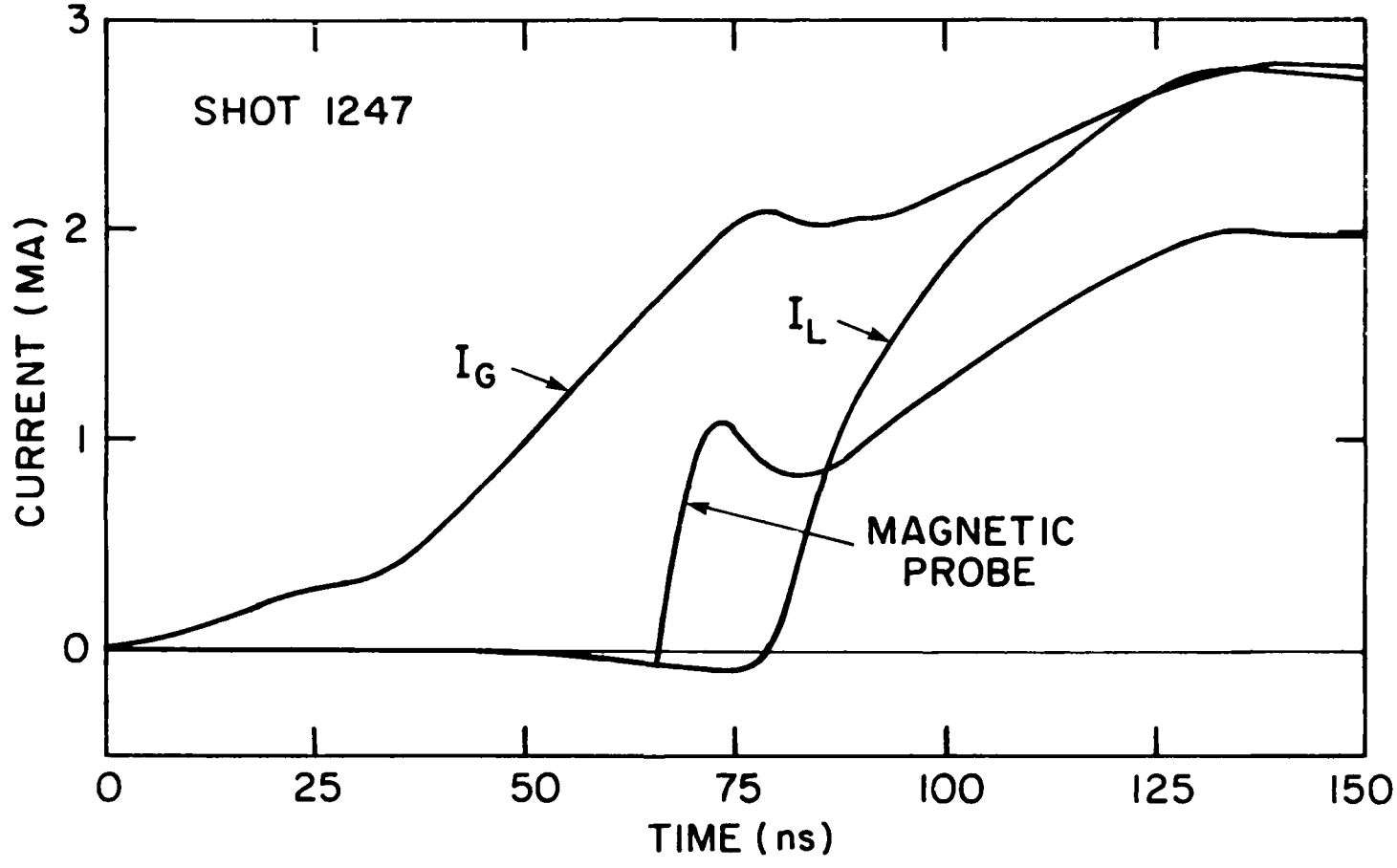

Fig. 29 Current measurements from the Blackjack 5/PBFA II experiment. The magnetic probe is located 2 cm from the load side of the 12-cm long switch. (Data from ref. 19).

Data from time resolved photographic, spectroscopic, microwave, and electric probe measurements present a consistent picture of the initial plasma conditions. These measurements give the approximate values that have been used by NRL in successfully modeling the PEOS. The plasma is primarily doubly ionized carbon, $\langle Z \rangle = 2$, with an electron temperature of $T_e \simeq 4\text{-}8$ eV. The electron density increases in time and reaches $\simeq 6 \times 10^{13}$ cm^{-3} at 7-10 cm from the source 2 μs after the source is fired. At this time the bulk of the inter-electrode plasma is unaffected by the presence of the metal electrode surfaces. The density between the surfaces continues to increase and temperature decrease with time to $n_e \simeq 3 \times 10^{14}$ cm^{-3} and $T_e \simeq 5$ eV at $\simeq 6$ μs after the source is fired. Also, lower charge state carbon (C and C^+) and neutral hydrogen evolve from the electrode surfaces $\simeq 1.5$ μs after the source is fired and begin to diffuse into the inter-electrode region at $\simeq 1$ cm/μs changing, among other parameters, $\langle Z \rangle$. Note that the Faraday cup signals begin to decrease at $\simeq 2$ μs after the plasma source is fired, in apparent contradiction to the other diagnostics.

The switch conduction current was studied by varying the switch geometry and conduction time. The measured peak current conducted by the PEOS scales approximately in accordance with Eq. (11) using the values for the plasma parameters measured in the bulk of the plasma. For the case investigated here, the peak conduction current was, to first order, independent of conduction time.

Spacially and temporally resolved magnetic probe measurements reveal that over a wide range of parameters the switch current is azimuthally

symmetric and flows in a broad ($>>c/\omega_{pe}$), predominately radial current channel for delay times when fast switching is observed. The radial current channel front moves steadily through the switch until its leading edge reaches the load side of the switch plasma, whereupon the switch begins opening into a short circuit load. For usual operating conditions the magnitude and constancy of the rate of current channel penetration are incompatible with associated mass motion. With longer delay times, when the opening is degraded, the discharge is not symmetric. This may be related to the change in plasma parameters. For delay times where no switching occurs, the current channel never reaches the load side of the switch plasma.

V. ACKNOWLEDGEMENTS:

We greatefully acknowledge the expert technical assistance of P. Bell and R. Boller. Dr. P. Ottinger provided the calculations for Fig. 18. We also wish to acknowledge Drs. G. Cooperstein, Shyke A. Goldstien, and R.A. Meger for their encouragement.

This work was supported in part by the Office of Naval Research, the Department of Energy, and the Defense Nuclear Agency.

REFERENCES

1. R.J. Commisso, G. Cooperstein, R.A. Meger, J.M. Neri, P.F. Ottinger, and B.V. Weber, NRL Memorandum Report 5560 (1985), to be published in Advances in Pulsed Power Technology, A. Guenther and M. Kristiansen, Eds., Plenum Press, 1987, and references there in.

2. C.W. Mendel, Jr., D.M. Zagar, G.S. Mills, S. Humphries, Jr., and S.A. Goldstein, Rev. Sci. Instrum. 51, 1641, (1980).

3. B.V. Weber, J.R. Boller, R.J. Commisso, J. Grossmann, D.D. Hinshelwood, R.A. Meger, J.M. Neri, W.F. Oliphant, P.F. Ottinger, T.J. Renk, S.J. Stephanakis, and F.C. Young, Fifth IEEE Pulsed Power Conference, Arlington, VA (1985), IEEE Cat. No. 85-C2121-2, p. 440.

4. R.A. Meger, R.J. Commisso, G. Cooperstein and Shyke A. Goldstein, Appl. Phys. Lett. 42, 943 (1983).

5. J.M. Neri, R.J. Commisso, and R.A. Meger, Bull. Am. Phys. Soc. 27, 1054 (1982).

6. J.M. Neri, R.J. Commisso, S.A. Goldstein, R.A. Meger, P.F. Ottinger, B.V. Weber and F.C. Young, 1983 IEEE International Conference on Plasma Science, San Diego, CA (1983), IEEE Cat. No. 83CH1947-3, p. 124.

7. R.W.P. McWhirter, in Plasma Diagnostic Techniques, R.H. Huddlestone and S.L. Leonard, Eds., Academic Press, New York, 1965, ch. 5.

8. D. Dustin, private communication.

9. C.B. Wharton in Plasma Diagnostic Techniques, R.H. Huddlestone and S.L. Leonard, Eds., Academic Press, New York, 1965, ch. 11.

10. M.A. Heald and C.B. Wharton, Plasma Diagnostics with Microwaves, Wiley, New York, 1965.

11. F.F. Chen, in Plasma Diagnostic Techniques, R.H. Huddelstone and S.L. Leonard, Eds., Academic Press, New York, 1965, ch. 4.

12. Paul M. Chung, Lawrence Talbot, Kenell J. Touryan, Electric Probes in Stationary and Flowing Plasmas, Springer Verlag, NY, 1975, p.29.

13. H. Bluhm, K.Bohnell, H.V.Karow, D. Rusch, and H. Schulken, 1985 IEEE International Conference on Plasma Science, Pittsburgh, PA (1985), IEEE Cat. No 85CH2199-8, p.80.

14. D.D. Hinshelwood, J.R. Boller, R.J. Commisso, G. Cooperstein, R.A. Meger, J.M. Neri, P.F. Ottinger, and B.V. Weber, Appl. Phys Lett. 49, 1635 (1986).

15. B.V. Weber, R.J. Commisso, R.A. Meger, J.M. Neri, W.F. Oliphant, and P.F. Ottinger, Appl. Phys Lett. 45, 1043 (1984).

16. B.V. Weber, D.G. Colombant, R.J. Commisso, G. Cooperstein, J.M. Grossmann, D.D. Hinshelwood, R.M. Kulsrud, R.A. Meger, D. Mosher, J. M. Neri, W.F. Oliphant, and P.F. Ottinger, 6th International Conference on High Power Particle Beams, Kobe, Japan (1986) C. Yamanaka, Ed., p. 851.

17. B.V. Weber, R.J. Commisso, J.M. Grossmann, D.D. Hinshelwood, R.A. Meger, J.M. Neri, W. F. Oliphant, and P.F. Ottinger, Bull. Am Phys. Soc. 30, 1447 (1985).

18. B.V. Weber, R.J. Commisso, D.D. Hinshelwood, R.A. Meger, J.M. Neri, W.F. Oliphant, P.F. Ottinger, T.J. Renk, Bull. Am. Phys. Soc. 29, 1206 (1984).

19. R. Stinnett, private communication.

DISTRIBUTION LIST

JOINT DNA AND DOE SPONSORED WORK
4 AUGUST 1987

Director
Defense Nuclear Agency
Washington, DC 20305
Attn: TISI Archieves 1 copy
TITL Tech. Library 3 copies
J.Z. Farber (RAEV) 1 copy
J. Fisher (RAEV) 1 copy
M. Herbert 1 copy
P. Filios (RAEV) 1 copy

U.S. Department of Energy
Division of Inertial Fusion
Washington, DC 20545
Attn: L.E. Killion 1 copy
M. Sluyter 1 copy
R.L. Schriever 1 copy

U.S. Department of Energy
Office of Classification
Washington, DC 20545
Attn: Robert T. Duff 1 copy

U.S. Department of Energy
Nevada Operations Office
Post Office Box 14100
Las Vegas, NV 89114 2 copies

U.S. Department of Energy
P.O. Box 62
Oak Ridge, TN 37830 2 copies

Air Force Office of Scientific Research
Physics Directorate
Bolling AFB, DC 20332
Attn: H. Pugh 1 copy
R.J. Barker 1 copy

Air Force Weapons Laboratory, AFSC
Kirtland AFB, NM 87117
Attn: NTYP (W.L. Baker) 1 copy

Atomic Weapons Research Establishment
Building H36
Aldermaston, Reading RG 7 4PR
United Kingdom
Attn: J.C. Martin 1 copy

Boeing Company
P.O. Box 3707
Seattle, WA 98124
Attn: Aerospace Library 1 copy

Brookhaven National Laboratory
Upton, NY 11973
Attn: A.F. Maschke 1 copy

BMO/EN
Norton AFB, CA
Attn: ENSN 1 copy

Commander
Harry Diamond Laboratory
2800 Powder Mill Rd.
Adelphi, MD 20783
(CNWDI-INNER ENVELOP: ATTN:DELHD-RBH)
Attn: DELHD-NP 1 copy
DELHD-RCC- 1 copy
J.A. Rosando
DRXDO-RBH - J. Agee 1 copy
DRXDO-TI - Tech Lib 1 copy

Cornell University
Ithaca, NY 14850
Attn: D.A. Hammer 1 copy
R.N. Sudan 1 copy

Defense Technical Information Center
Cameron Station
5010 Duke Street
Alexandria, VA 22314
Attn: T.C. 2 copies

JAYCOR, Inc.
205 S. Whiting Street
Alexandria, VA 22304
Attn: D.D. Hinshelwood 1 copy
B.V. Weber 1 copy

Kaman Tempo
816 State Street (P.O. Drawer QQ)
Santa Barbara, CA 93102
Attn: DASIAC 1 copy

KMS Fusion, Inc.
3941 Research Park Drive
P.O. Box 1567
Ann Arbor, MI 48106
Attn: Alexander A. Glass 1 copy

Lawrence Berkeley Laboratory
Berkeley, CA 94720
Attn: D. Keefe 1 copy

Lawrence Livermore National Laboratory
P.O. Box 808
Livermore, CA 94550
Attn: Tech Info Dept L-3 1 copy
D.J. Meeker 1 copy
R.E. Batzel/
J. Kahn, L-1 1 copy
J.L. Emmett, L-488 1 copy
E. Storm, L-488 1 copy
W.F. Krupke, L-488 1 copy
J. Lindl, L-477 1 copy

Los Alamos National Laboratory
P.O. Box 1663
Los Alamos, NM 87545
Attn: M. Gillispie/
Theo. Div. 1 copy
S.D. Rockwood, ICF
Prog. Mgr. DAD/IF
M/S 527 6 copies

Massachusetts Institute of Technology
Cambridge, MA 02139
Attn: R.C. Davidson 1 copy
G. Bekefi 1 copy

Maxwell Laboratories, Inc.
9244 Balboa Avenue
San Diego, CA 92123
Attn: M. Montgomery 1 copy

Mission Research Corporation
1400 San Mateo Blvd. SE
Albuquerque, NM 87108
Attn: B.B. Godfrey 1 copy

National Science Foundation
Mail Stop 19
Washington, DC 20550
Attn: D. Berley 1 copy

Naval Research Laboratory
Washington, DC 20375-5000
Attn: Code/Name

2628	TID Distrib.	22 copies
1001	T. Coffey	1 copy
4000	W. Ellis	1 copy
4040	J. Boris	1 copy
4700	S. Ossakow	26 copies
4701	I. Vitkovitsky	1 copy
4704	C. Kapetanakos	1 copy
4720	J. Davis	1 copy
4730	S. Bodner	1 copy
4740	W. Manheimer	1 copy
4760	B. Robson	1 copy
4770	G. Cooperstein	10 copies
4770.1	F. Young	1 copy
4770.2	R. Commisso	1 copy
4771	P. Ottinger	1 copy
4771	J. Grossmann	1 copy
4771	J. Neri	1 copy
4773	R. Meger	1 copy
4773	S. Stephanakis	1 copy
4790	D. Colombant	1 copy
4790	I. Haber	1 copy
4790	M. Lampe	1 copy
6682	D. Nagel	1 copy

Physics International Co.
2700 Merced Street
San Leandro, CA 94577
Attn: C. Stallings 1 copy

Pulse Sciences, Inc.
1615 Broadway, Suite 610
Oakland, CA 94612
Attn: S. Putnam 1 copy

R&D Associates
Suite 500
1401 Wilson Blvd.
Arlington, VA 22209
Attn: P.J. Turchi 1 copy

SAI
8400 W. Park Ave.
McLean, VA 22102
Attn: A. Drobot 1 copy

R&D Associates
P.O. Box 9695
Marina Del Rey, CA 90291
Attn: C. MacDonald 1 copy

Sandia National Laboratories
P.O. Box 5800
Albuquerque, NM 87185
Attn: D.L. Cook / 1260 5 copies
T. Martin / 1250 1 copy
J. Vandevender/1200 1 copy

Spire Corporation
P.O. Box D
Bedford, MA 01730
Attn: R.G. Little 1 copy

Stanford University
SLAC
P.O. Box 4349
Stanford, CA 94305
Attn: W.B. Herrmannsfeldt 1 copy

University of California
Irvine, CA 92717
Attn: N. Rostoker 1 copy

University of Rochester
250 East River Road
Rochester, NY 14623
Attn: J. Eastman 1 copy

University of Washington
Dept. of Nuclear Engineering
BF-10
Seattle, WA 98115
Attn: F. Ribe 1 copy

NRL Code 1220 1 copy

Records 1 copy

DIRECTOR OF RESEARCH
U.S. NAVAL ACADEMY
ANNAPOLIS, MD 21402
2 COPIES